



Jian, D., Ma, Z., Chen, L., Duan, J., Mitchell, D., Zheng, Z., Lv, M., & Zhang, H. (2020). Effects of 1.5°C and 2°C of warming on regional reference evapotranspiration and drying: A case study of the Yellow River Basin, China. *International Journal of Climatology*.
<https://doi.org/10.1002/joc.6667>

Peer reviewed version

Link to published version (if available):
[10.1002/joc.6667](https://doi.org/10.1002/joc.6667)

[Link to publication record in Explore Bristol Research](#)
PDF-document

This is the author accepted manuscript (AAM). The final published version (version of record) is available online via Wiley at <https://rmetsonline.wiley.com/doi/abs/10.1002/joc.6667?af=R>. Please refer to any applicable terms of use of the publisher.

University of Bristol - Explore Bristol Research

General rights

This document is made available in accordance with publisher policies. Please cite only the published version using the reference above. Full terms of use are available:
<http://www.bristol.ac.uk/red/research-policy/pure/user-guides/ebr-terms/>

1 **Reduced Reference Evapotranspiration and Aridity from 0.5°C**
2 **Less Warming in the Yellow River Basin, China**

3 **Dongnan Jian^{1,2}, Zhuguo Ma^{1,2}, Daniel Mitchell³, Liang Chen¹, Jianping Duan¹,**
4 **Haixin Zhang^{1,2}, Ziyang Zheng¹, Meixia Lv¹**

5 ¹ CAS Key Laboratory of Regional Climate-Environment for Temperate East Asia,
6 Institute of Atmospheric Physics, Chinese Academy of Sciences, Beijing, China,

7 ² University of Chinese Academy of Sciences, Beijing, China

8 Corresponding author: Zhuguo Ma (mazg@tea.ac.cn)

9 ³School of Geographical Sciences, University of Bristol, Bristol, UK

10 **Key Points:**

- 11 • Changes in the reference evapotranspiration and aridity in the Yellow River
12 Basin in response to warmings of 1.5°C and 2°C were quantified
- 13 • Compared to the reference period, the reference evapotranspiration and aridity
14 increases in the 1.5 and 2 °C warmer worlds
- 15 • The reference evapotranspiration and aridity are lower in a 1.5 °C warmer
16 world than in a 2 °C warmer world

17 **Abstract**

18 In this study, the reference evapotranspiration (ET_o) in the Yellow River Basin (YRB)
19 during 1961–2017 was calculated by the Penman-Monteith method from observed
20 meteorological data, and the simulated ET_o in the reference period (2006-2015) and
21 with global warming levels of 1.5 and 2°C were calculated from the outputs of the
22 Half a degree Additional warming, Prognosis and Projected Impacts (HAPPI) project.
23 We found that the ET_o increased significantly during 1961-2017 in the central and
24 southern parts of the upper basin and western part of the middle basin, and it
25 decreased significantly in the northeastern portion of the upper basin and the eastern
26 portion of the middle basin and lower basin. The multiyear average ET_o of the YRB
27 projected by CAM4-2degree, ECHAM6-3-LR, MIROC5 and NorESM1-HAPPI
28 increases by 49.1, 41.0, 30.9 and 47.6 mm at 1.5°C warming, respectively, and 77.9,
29 76.6, 93.7 and 80.6 mm at 2°C warming, respectively, compared to the reference
30 period. The increment in the ET_o exceeds the increment of the precipitation in
31 warmer worlds. This phenomenon is likely to intensify the aridity in the YRB,
32 especially at 2°C warming world. Limiting global warming to 1.5°C is the most
33 beneficial to the North China Plain, southern part of Hetao Plain and Ordos Plateau
34 and northwestern part of the Loess Plateau that ET_o can be reduced over 30mm in
35 these regions. The main factors contributing to the increase in ET_o at the two
36 warming levels are the maximum temperature (tasmax), downwelling shortwave
37 radiation (rsds), and relative humidity (hurs).

38 **1 Introduction**

39 The Yellow River Basin (YRB) has played a significant role in China's long
40 history, food production, and socioeconomic development (Cai and Rosegrant, 2004;
41 Zhu et al., 2004). It has been reported that drought has occurred frequently in the
42 YRB and has had socioeconomic and environmental effect (She and Xia, 2013). The
43 drought that extended from the late 1920s to the early 1930s impacted approximately
44 20 million people and led to over 3 million deaths (Xie and Fu, 2004). The water
45 crisis of the YRB has come into notice worldwide, especially the serious drying up of
46 the main river in the lower basin that occurred during the 1990s (Cong et al., 2009).
47 The drying up recorded at the Lijin station first started in 1972 and 20 instances of the
48 river drying up occurred between this year and 1997. The most serious instance
49 happened in 1997, when the area along the lower reaches dried up for 226 days over a
50 distance of 704 km (Ma, 2005). In addition, both the observed and natural runoffs of
51 the Yellow River showed decreasing trends during the last half century (Cong et al.,
52 2009; Cuo et al., 2013; Wang et al., 2013; Yan et al., 2013; Yang et al., 2004) due to
53 significant increases in the artificial water consumption (Cong et al., 2009; Wang et
54 al., 2016; Yang et al., 2004). The water utilization for agriculture, industry, and
55 households in the past decade seriously impacted the environmental and ecological
56 water requirements (Cai and Rosegrant, 2004; Shiau et al., 2007; Zhu et al., 2004).
57 With the growing economy and increasing population, the irrigation areas also
58 progressively expanded from 800 thousand hectares in 1949 (Fu et al., 2004) to 4424
59 thousand hectares by 2007 (YRCC, 2007). The reference evapotranspiration (ET_o) is

60 a good proxy to measure the drought conditions in environmental, hydrological and
61 agricultural systems (Sun et al., 2015; Trenberth et al., 2013; Vicente-Serrano et al.,
62 2012, 2015). An increase in evapotranspiration could have serious repercussions on
63 water resources (McVicar et al., 2007). It has been proven that the most sensitive
64 climate factor for naturalized streamflow in the YRB is the potential
65 evapotranspiration (Lv et al., 2018). Its estimation and projection are thus crucial to
66 understanding the water cycle of a basin or region (Jian et al., 2018; Su et al., 2017).

67 The evapotranspiration from a reference surface that is not short of water is the
68 reference evapotranspiration. The reference surface is a hypothetical grass reference
69 crop with an assumed crop height of 0.12 m, a fixed surface resistance of 70 s m^{-1}
70 and an albedo of 0.23 (Allen et al., 1998). The reference surface is very similar to an
71 extensive surface of green, well-watered grass of uniform height, actively growing
72 and completely shading the ground (Allen et al., 1998). The E_{To} is an important
73 parameter for the characterization of the hydrological cycle and is affected only by
74 climatic parameters (Allen et al., 1998). It indicates an upper limit for the actual
75 evapotranspiration in a humid climate, while it denotes the total available energy for
76 actual evapotranspiration in an arid climate (Gong et al., 2006). It is the most
77 important factor to consider in calculating the actual evapotranspiration (Wang et al.,
78 2017; Xu and Singh, 2004). It is also an input to irrigation system and hydrological
79 models and is important for the assessment of the hydrological impact of climate
80 change (Xu et al., 2006). With climate warming, it was expected that the
81 evapotranspiration will also increase (Roderick and Farquhar, 2002). However,

82 declines in the observed pan evaporation and ETo have been observed in many
83 regions around the world by a great deal of studies, for example, in the United States
84 and the former Soviet Union (Golubev et al., 2001; Peterson et al., 1995), India
85 (Bandyopadhyay et al., 2009; Chattopadhyay and Hulme, 1997; Jhajharia et al.,
86 2009), China (Liu et al., 2004), Australia (Roderick and Farquhar, 2004), Japan (Jun
87 et al., 2004), and the Canadian Prairies (Burn and Hesch, 2007). Such a contrast
88 between the expectation and observation is called the “evaporation paradox”
89 (Roderick and Farquhar, 2002). Explanations for this phenomenon included the
90 decreasing solar radiation or sunshine duration (Jhajharia et al., 2009; Liu et al., 2004;
91 Peterson et al., 1995; Roderick and Farquhar, 2002; Xu et al., 2006) and wind speed
92 (Burn and Hesch, 2007; Roderick et L., 2007), increasing relative humidity
93 (Bandyopadhyay et al., 2009; Chattopadhyay and Hulme, 1997), and the
94 complementary relationship between the actual and potential evapotranspiration
95 (Hobbins, 2004). Some researchers found that the ETo increased in some areas of the
96 upper and middle basins of YRB (Liu et al., 2010; Wang et al., 2012). The ETo is also
97 projected to increase over the 21st century on the Loess Plateau (Li et al., 2012).
98 Methods for the quantification of the ETo in a basin or region at specific warming
99 targets are lacking. The issue of how the ETo will change in a warmer world and
100 therefore give rise to drier or wetter conditions in the YRB is worth discussion due to
101 its great socioeconomic impact.

102 The Paris Agreement was adopted on the 12th of December 2015 at the United
103 Nations Framework Convention on Climate Change (UNFCCC) and provides a

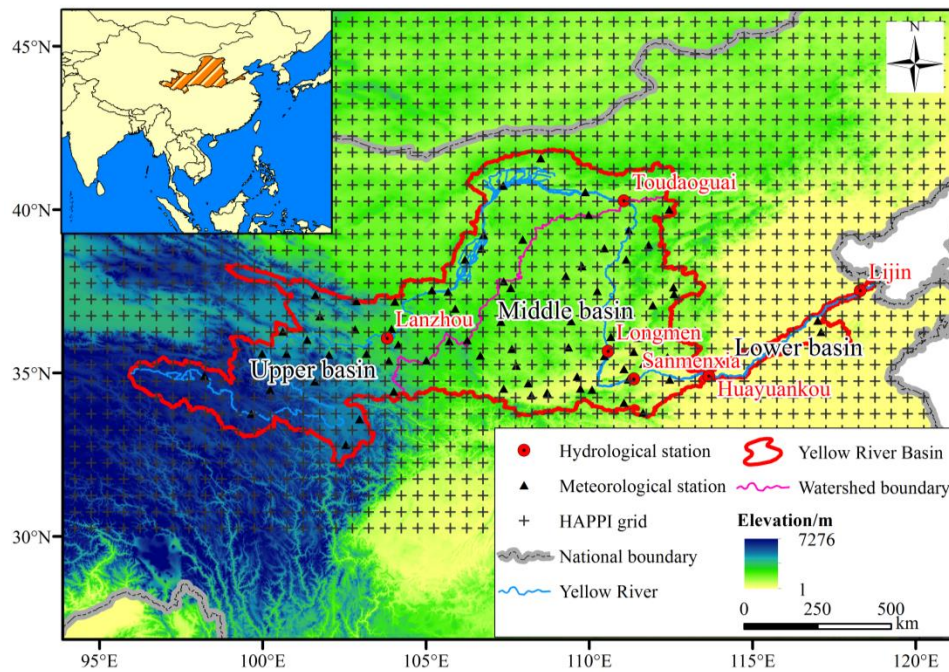
104 framework for global actions to address climate change. The 2015 Paris Agreement
105 reflected a commitment to “holding the increase in the global average temperature to
106 well below 2.0 °C above pre-industrial levels and pursuing efforts to limit the
107 temperature increase to 1.5 °C, recognizing that this would significantly reduce the
108 risks and impacts of climate change”. Since the Paris Agreement, there has been a call
109 for assessing the effects from global warming of 1.5 and 2 °C (Mitchell et al., 2016;
110 Schleussner et al., 2016). An IPCC special report on the impacts of global warming of
111 1.5 °C suggested that the climate-related risks in natural and human systems are lower
112 for a global warming of 1.5°C than for 2°C (IPCC, 2018). Most published results have
113 been based on the existing Coupled Model Intercomparison Project (CMIP5) (Taylor
114 et al., 2012), which was not specifically designed for the assessment of the 1.5 and
115 2°C warming worlds (Mitchell et al., 2016). For that reason, HAPPI was proposed to
116 provide a framework to assess the impacts at the 1.5°C warming level and the impacts
117 avoided compared to those at 2°C (Mitchell et al., 2017). Researchers assessed
118 changes in the runoff and water resources (Zhai et al, 2018), agricultural impacts
119 (Ruane et al., 2018; Schleussner et al., 2018), climate extreme (Baker et al., 2018;
120 Lewis et al, 2017; Seneviratne et al., 2018; Wehner et al., 2018), land–climate
121 feedbacks and land-use forcing (Seneviratne et al., 2018) for global warming levels of
122 1.5 and 2 °C by using HAPPI outputs, but there has been limited discussion on the
123 impacts of specific warming targets on a region or basin.

124 Here, the ETo of the YRB from 1961 to 2017 was calculated by Penman-
125 Monteith equation based on observed meteorological data. We evaluated the

126 simulations of HAPPI of the ETo by comparing the multiyear average and spatial
 127 pattern of the ETo. Using the HAPPI outputs, we examine how much the ETo may
 128 change under stabilized global mean temperature increases of 1.5 and 2°C above
 129 preindustrial levels in the YRB and estimate the beneficial reduction that will be
 130 achieved by limiting global warming to 1.5°C, focusing on the potential changes of
 131 aridity. We calculate the relative contributions of climatic variables to the change in
 132 ETo at two warming levels. The results are expected to contribute to an understanding
 133 of the regional patterns in ETo under two global warming levels.

134 **2 Materials and Methods**

135 2.1 Study area



136
 137 Fig. 1. Location of the YRB and its subbasin as well as of the hydrological and meteorological

138 stations and the HAPPI grid

139

140 The Yellow River (Fig. 1), originating from the Qinghai-Tibet Plateau, is the
141 second-longest river in China, with a length of 5464 km, and it covers a drainage area
142 of 79.5×10^4 km² (YRCC., 2015). The YRB supports a population of approximately
143 110 million people and has 12.6×10^6 ha of cultivated land (Shiau et al., 2007). From
144 northwest to southeast, the climate of the YRB is characterized by an arid, semiarid
145 continental monsoon climate and semi-humid climate (Wang and Peng, 2017). The
146 YRB covers three typical landforms, namely, the Tibetan Plateau (2000-5000 m), the
147 Loess Plateau (500-2000 m), and the alluvial plain (Yang et al., 2004). The tributaries
148 upstream of Lanzhou station flow into the main channel of the Yellow River and
149 account for 62% of the runoff of the whole basin (Wang and Peng, 2017). There is a
150 slow-flowing stream from Lanzhou to Toudaoguai stations, and the basin valley and
151 Hetao Plain are located in this section. Downstream of Toudaoguai station, the
152 Yellow River flows through the Loess Plateau, where there is serious water loss and
153 soil erosion, and 90% of the sediment delivered to the Yellow River comes from here
154 (Tang et al., 1991). “Revegetation schemes” and “engineering methods” were used to
155 reduce the sediment loads reaching the Yellow River (McVicar, 2007). From
156 Sanmenxia to Huayuankou stations, the river has many tributaries, and the slope of
157 river is steep, helping the production of runoff and confluence. Downstream of
158 Huayuankou station is the North China Plain. Large quantities of sediment are carried
159 by mudflow from the plateau and cause serious silting and aboveground rivers in the
160 lower reaches (Douglas, 1989; Shi and Shao, 2000). Issues of water shortages and
161 environmental deterioration have become very serious in the YRB and the prime

162 water-related issues in this basin are soil erosion and sedimentation, flooding, and
163 water shortages (Wang and Peng, 2004). Flooding and drought have negatively
164 impacted the agriculture and people's lives in the lower basin and caused huge
165 economic losses and human death and injury (Wang and Peng, 2017).

166 2.2 Data

167 In current study, daily observed data from 80 meteorological stations (Fig. 1)
168 in the YRB during the period of 1961-2017, including the air temperature,
169 precipitation, maximum /minimum air temperature, relative humidity, atmospheric
170 pressure, wind speed (10-m height), and sunshine duration, were obtained from the
171 National Meteorological Information Center of the China Meteorological
172 Administration. The data quality was checked by means of climatic boundary values,
173 extreme values, and internal consistency. Stations missing more than 5% of the days
174 in a year were rejected. The missing daily records of a station were filled by the
175 multiyear averaged values of the station.

176 The discharge data in this study included naturalized and observed
177 streamflows at a total of 6 hydrological stations (Fig. 1). Annual data were available
178 from 1961 to 2010 for the Lanzhou, Toudaoguai, Longmen, Sanmenxia, Huayuankou
179 and Lijin stations. Annual data were obtained from the Yellow River Conservancy
180 Commission, which is the sole authority in China in charge of quality control and the
181 release of water data (Fu et al., 2004). Given the intense human activities in the YRB,
182 naturalized streamflow data without human intervention were also considered in the

183 current study. The naturalized and observed streamflows are different in their
184 influence from human activities, such as reservoir regulation, interbasin water
185 diversion, and water withdrawal for irrigation, industrial, and domestic uses (Fu et al.,
186 2004; Lv et al., 2017). The locations of the meteorological stations, the hydrological
187 stations, and the subbasins are shown in Fig. 1.

188 The climate output data used in this study are projections from the Half a
189 degree Additional warming, Projections, Prognosis and Impacts project (HAPPI;
190 Mitchell et al., 2017). HAPPI provides climate data to assess how the climate,
191 especially extreme weather, might be different from the present in the world under
192 conditions 1.5 and 2.0°C warmer than pre-industrial conditions (Mitchell et al., 2017).
193 HAPPI is based on the atmospheric components of CMIP5 models forced by
194 prescribed sea surface temperature (SST) and sea ice concentrations (Mitchell et al.,
195 2017). Four GCMs (Tab. 1), CAM4-2degree, ECHAM6-3-LR, MIROC5, and
196 NorESM1-HAPPI, were used in the current study and were bias-corrected using the
197 Inter-Sectoral Impact Model Intercomparison Project (ISIMIP2b) (Lange, 2018). The
198 bias correction was applied to each ensemble members of each of the four HAPPI
199 GCMs and has significantly improved the ensemble mean performance while
200 preserving the ensemble variability (Döll et al., 2018). The reference period of the
201 HAPPI experiment is the most recent decade from 2006–2015. The 1.5 and 2°C
202 warmer than pre-industrial (1861-1880) experiment is based on the RCP2.6
203 experiment from 2106 to 2115 and the weighted combination of the RCP2.6 and
204 RCP4.5 experiments from 2106 to 2115, respectively. The model outputs include the

205 air temperature (tas), maximum (tasmax)/minimum air temperature (tasmin), relative
 206 humidity (hurs), wind speed (sfcWind), precipitation (prec), and downwelling
 207 shortwave (rsds)/ longwave radiation (rlds).

208 Tab. 1. Details of the HAPPI models used in this study. Note the horizontal resolution was
 209 changed from the modal native resolution during the ISI-MIP bias correction method.

| GCM | Ensemble members: allhist/plus1.5/plus2.0 | Horizontal Resolution |
|---------------|---|-----------------------|
| CAM4-2degree | 20/20/20 | 0.5°×0.5° |
| ECHAM6-3-LR | 20/20/20 | 0.5°×0.5° |
| MIROC5 | 10/10/10 | 0.5°×0.5° |
| NorESM1-HAPPI | 20/20/20 | 0.5°×0.5° |

210 2.3Method

211 The Penman–Monteith method was applied in the current study to calculate
 212 the ETo. It has been recommended by the Food and Agricultural Organization (FAO)
 213 as the best method to determine the ETo (Allen et al., 1998).

$$214 \quad ET_o = \frac{0.408\Delta(R_n - G) + \gamma \frac{900}{T + 273} u_2 (e_s - e_a)}{\Delta + \gamma(1 + 0.34u_2)} \quad (1)$$

215 where Rn represents the net radiation at the crop surface (MJ m⁻² day⁻¹), G is
 216 the soil heat flux density (MJ m⁻² day⁻¹), u₂ is the wind speed at a 2 m height (m s⁻¹),
 217 e_s is the saturation vapor pressure (kPa), e_a is the actual vapor pressure (kPa), e_s –
 218 e_a is the saturation vapor pressure deficit (kPa), Δ is the slope vapor pressure curve
 219 (kPa °C⁻¹), and γ is a psychrometric constant (kPa °C⁻¹). The daily soil heat flux is
 220 regarded as 0 in the current study (Allen et al., 1998).

221 Detailed algorithms of the above variables were according to Allen et al.
222 (1998). Observed meteorological factors, including the maximum/minimum air
223 temperature, relative humidity, atmospheric pressure, sunshine duration, and wind
224 speed, were used to calculate the ETo. HAPPI outputs, including the tasmax, tasmin,
225 hurs, sfcWind and rsds, were involved in computing the ETo. In the current study, the
226 air temperature was computed as the average of the tasmax and tasmin, as was
227 recommend by the FAO (Allen et al., 1998). The HAPPI outputs do not include the
228 atmospheric pressure and the sunshine duration, which are necessary to calculate the
229 psychrometric constant and net radiation. The effect of the atmospheric pressure is
230 small in the calculation of the ETo (Allen et al., 1998). A simplification of the ideal
231 gas law, assuming 20°C for a standard atmosphere, was used to calculate P (Allen et
232 al., 1998):

$$P = 101.3 \left(\frac{293 - 0.0065z}{293} \right)^{5.26} \quad (2)$$

234 Where P is the atmospheric pressure (kPa) and z is the elevation above sea
235 level (m).

236 HAPPI provides the rsds and rlds data, but it does not have upwelling
237 longwave radiation data. We used the following equations to calculate the net
238 radiation. The net shortwave radiation R_{ns} is expressed in the follow equation:

$$R_{ns} = (1 - \alpha)R_s \quad (3)$$

240 Where R_{ns} is the net solar or shortwave radiation ($\text{MJ m}^{-2} \text{ day}^{-1}$), α is the
241 albedo or canopy reflection coefficient, which is 0.23 for the hypothetical grass

242 reference crop (dimensionless), and R_s is the downwelling solar radiation ($\text{MJ m}^{-2} \text{ day}^{-1}$).
 243

244 The extraterrestrial radiation R_a can be estimated from the solar constant, the solar
 245 declination and the time of the year by:

$$246 \quad R_a = \frac{12(60)}{\pi} G_{SC} d_r [\omega_s \sin(\varphi) \sin(\delta) + \cos(\varphi) \cos(\delta) (\sin(\omega_s))] \quad (4)$$

247 Where R_a is the extraterrestrial radiation ($\text{MJ m}^{-2} \text{ day}^{-1}$), G_{SC} is the solar
 248 constant = $0.0820 \text{ MJ m}^{-2} \text{ min}^{-1}$, d_r is the inverse relative Earth-Sun distance
 249 (Equation 5), δ is the solar declination (Equation 6) (rad), ω_s is the sunset hour angle
 250 (Equation 7) (rad), and φ is the latitude (rad).

251 The inverse relative Earth-Sun distance (d_r), the solar declination (δ) and
 252 sunset hour angle (ω_s) are given by:

$$253 \quad d_r = 1 + 0.033 \cos\left(\frac{2\pi}{365} J\right) \quad (5)$$

$$254 \quad \delta = 0.409 \sin\left(\frac{2\pi}{365} J - 1.39\right) \quad (6)$$

$$255 \quad \omega_s = \arccos[-\tan(\varphi) \tan(\delta)] \quad (7)$$

256 Where J is the number of the day in the year between 1 and 365 or 366.

$$257 \quad R_{nl} = \sigma \left[\frac{T_{max,K}^4 + T_{min,K}^4}{2} \right] (0.34 - 0.14 \sqrt{e_a}) \left(1.35 \frac{R_s}{R_{so}} - 0.35 \right) \quad (8)$$

258 Where R_{nl} is the net outgoing longwave radiation ($\text{MJ m}^{-2} \text{ day}^{-1}$), σ is the
 259 Stefan-Boltzmann constant ($4.903 \times 10^{-9} \text{ MJ K}^{-4} \text{ m}^{-2} \text{ day}^{-1}$), $T_{max,K}$ is the maximum
 260 absolute temperature during the 24-hour period ($\text{K} = ^\circ\text{C} + 273.16$), $T_{min,K}$ is the
 261 minimum absolute temperature during the 24-hour period ($\text{K} = ^\circ\text{C} + 273.16$), e_a is the
 262 actual vapor pressure (kPa), R_s/R_{so} is the relative shortwave radiation (limited to
 263 ≤ 1.0), and R_{so} is the clear-sky radiation (Equation 9) ($\text{MJ m}^{-2} \text{ day}^{-1}$).

264 The calculation of the clear-sky radiation (R_{so}) is as follows:

$$265 \quad R_{so} = (0.75 + 2 \times 10^{-5}z)R_a \quad (9)$$

266 Where z is the station elevation above sea level (m).

267 The net radiation (R_n) is the difference between the incoming net shortwave
268 radiation (R_{ns}) and the outgoing net longwave radiation (R_{nl}):

$$269 \quad R_n = R_{ns} - R_{nl} \quad (10)$$

270 To characterize the average difference between the ETos estimated by the
271 observed and simulated data at a grid point or region, the mean error (BIAS) is
272 estimated, which is defined as the positive or negative difference between the
273 observed (o) and simulated (s) means of the indicator. The equation for the BIAS is
274 given here:

$$275 \quad BIAS = \frac{1}{n} \sum_{i=1}^n (s_i - o_i) = \bar{s} - \bar{o} \quad (11)$$

276 To quantify the contribution of a climatic variable to the change of ETo at 1.5
277 and 2°C warming levels, a simple but practical method was employed as follows.
278 Taking 1.5°C warming as an example, (1) a climatic variable at the reference period
279 and other climatic variables at 1.5°C warming were considered to recalculate the ETo;
280 (2) the recalculated and original ETos at the 1.5°C warming level were compared and
281 (3) the difference was regarded as the influence of the change at 1.5°C warming by
282 that variable. The same method was applied to determine the contribution of a
283 climatic variable to the change of the ETo at 2°C warming level.

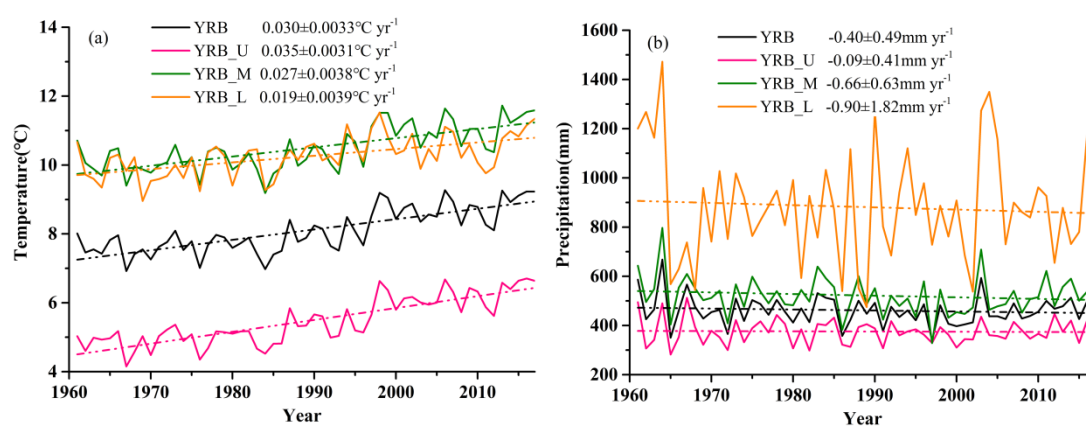
284 We used linear regression to analyze the trends in the climatic variables and
285 the nonparametric and Mann–Kendall (MK) test (Kendall, 1975; Mann, 1945) to
286 assess the significance. Inverse distance weighted (IDW) was used to interpolate the
287 ETos in meteorological stations to the same grid as HAPPI to evaluate the
288 performance of HAPPI on ETo. We assessed the relationships between the variables
289 by using Pearson correlation coefficients.

290 **3 Results**

291 3.1 Climatic and hydrologic characteristics

292 To have a comprehensive understanding of the long-term variability in the
293 climate and river discharge of the YRB, the annual average temperature and
294 precipitation and decadal average of the river discharges were examined. The YRB
295 has become increasingly warmer over the last 5–6 decades, in where the average air
296 temperature has increased at a rate of $0.035\pm 0.0031^{\circ}\text{C yr}^{-1}$ ($p<0.05$) during the period
297 of 1961-2017 (Fig. 2(a)). Especially in the upper basin, it has experienced an
298 increasing rate of $0.030\pm 0.0033^{\circ}\text{C yr}^{-1}$ ($p<0.05$). The air temperature has increased at
299 a rate of $0.027\pm 0.0038^{\circ}\text{C yr}^{-1}$ and $0.019\pm 0.0039^{\circ}\text{C yr}^{-1}$ ($p<0.05$) for the middle and
300 lower basins, respectively. Over the analysis period, the areal averaged precipitation
301 was highest in the lower basin (precipitation =881.3 mm), followed by the middle
302 basin (precipitation=521.8 mm), and upper basin (precipitation = 347.5 mm) (Fig. 2
303 (b)).

304 The precipitation of the YRB showed a slight decreasing trend, but the change
 305 is not significant. The areal average precipitation is approximately 461.3 mm for the
 306 whole basin. Overall, the precipitation for the whole, upper, middle and lower basins
 307 decreased at rates of 0.40 ± 0.49 , 0.09 ± 0.41 , 0.66 ± 0.63 and 0.90 ± 1.82 mm yr⁻¹,
 308 respectively, from 1961 to 2017.
 309



310

311 Fig. 2. Time series of: (a) annual temperature and (b) annual precipitation in the whole (black
 312 line), upper (pink line), middle (green line) and lower (orange line) basins from 1961 to 2017

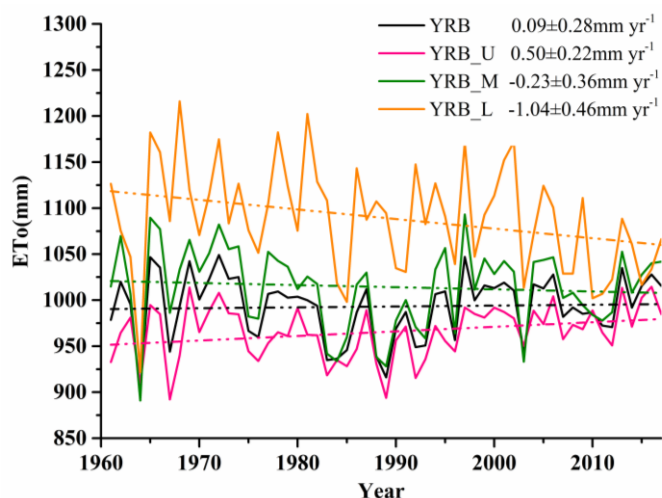
313 Ma et al. (2005) found that the natural runoff in the YRB changed decadal.
 314 Both the observed and natural runoffs recorded at Lanzhou, Toudaoguai, Longmen,
 315 Sanmenxia, Huayuankou and Lijin stations have the same generally decreasing trend.
 316 The natural and observed runoffs showed decreasing trends at all stations, and the
 317 observed runoff decreased more obviously. The average of the natural runoff during
 318 the 2000s compared to the 1960s decreased by 14.5%, 14.9%, 15.2%, 18.0%, 19.0%
 319 and 19.0% for the Lanzhou, Hekou, Longmen, Sanmenxia, Huayuankou and Lijin
 320 stations, respectively. During the last 5 decades, except for Lijin station, the observed

321 runoffs showed their smallest changes between the 1960s and the 1980s and their
 322 biggest changes from the 1990s to the 2000s. The runoff at Lijin station had a sharp
 323 decreasing trend from the 1970s, and has declined unceasingly since the 1990s. The
 324 averages of the observed runoff during the 2000s compared to the 1960s decreased by
 325 23.3%, 43.8%, 47.9%, 56.0%, 53.6% and 70.5% for Lanzhou, Toudaoguai, Longmen,
 326 Sanmenxia, Huayuankou and Lijin stations, respectively. Furthermore, as shown in
 327 Tab. 2, the difference between the observed and natural runoffs became wider,
 328 indicating there was a rapid increase in artificial water consumption, which
 329 aggravated the water resource crisis of the YRB.

330 Tab. 2. Decadal averages of observed/natural runoffs (10^8 m^3)

| | Lanzhou | Toudaoguai | Longmen | Sanmenxia | Huayuankou | Lijin |
|-----------|-------------|-------------|-------------|-------------|-------------|-------------|
| 1961-1970 | 355.8/355.7 | 270.2/335.7 | 337.1/363.1 | 464.5/469.9 | 522.8/526.0 | 527.4/527.6 |
| 1971-1980 | 318.5/322.9 | 232.6/306.9 | 280.4/329.3 | 350.7/401.6 | 373.8/439.8 | 294.7/441.4 |
| 1981-1990 | 338.7/358.4 | 241.9/343.6 | 279.9/365.5 | 376.9/457.5 | 419.0/506.5 | 293.5/508.1 |
| 1991-2000 | 254.2/277.0 | 150.4/259.1 | 189.6/280.1 | 225.4/342.7 | 236.9/379.5 | 119.2/381.1 |
| 2001-2010 | 273.0/304.3 | 151.9/285.8 | 175.5/307.8 | 204.2/385.5 | 242.7/426.0 | 155.4/427.6 |
| mean | 308.1/323.6 | 209.4/306.2 | 252.5/329.2 | 324.3/411.4 | 359.0/455.5 | 278.0/457.1 |

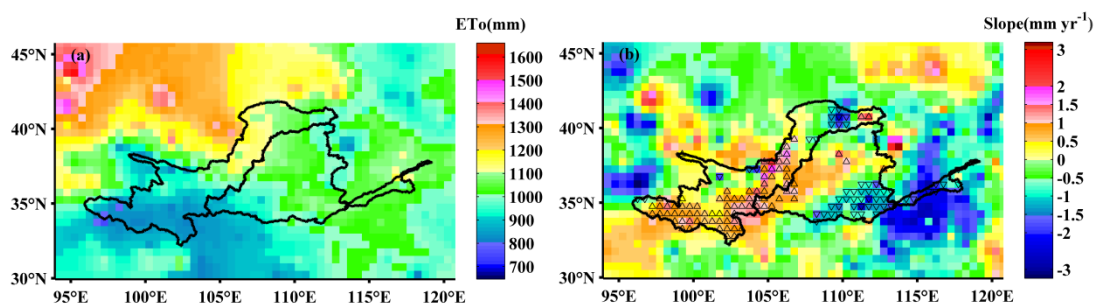
331 3.2 Observed ETo for the period 1961-2017



332

333 Fig. 3. Temporal variation of the annual ETo in the whole (black line), upper (pink line), middle
 334 (green line) and lower (orange line) basins of the YRB from 1961 to 2017

335 The temporal trends for the annual ETo during the period of 1961-2017 in the
 336 whole, upper, middle, and lower basins are shown in Fig. 3. The ETo in the whole and
 337 upper basins showed increasing trends for the period from 1961 to 2017. There was a
 338 significant ($p < 0.05$) increasing trend at a rate of $0.50 \pm 0.22 \text{ mm yr}^{-1}$ for the upper
 339 basin, and the ETo had an increasing but insignificant trend with a rate of 0.09 ± 0.28
 340 mm yr^{-1} for the whole basin. The ETos in the middle and lower basins showed
 341 significant ($p < 0.05$) declining trends at rates of -0.23 ± 0.36 and $1.04 \pm 0.46 \text{ mm yr}^{-1}$,
 342 respectively. The multiyear average ETos were approximately 993.0, 965.5, 1014.2,
 343 and 1089.2 mm for the whole, upper, middle, and lower basins, respectively.



344

345 Fig. 4. (a) Spatial distribution of the annual ETo in the YRB from 1961 to 2017. (b) Annual trend

346 slopes and the MK test result (at the 99% and 95% confidence levels) of the ETo during 1961–

347 2017. The colorbar indicates the trend slope of the ETo. The red upward and blue downward

348 triangles indicate significant (95% confidence) increasing and decreasing tendencies, respectively,

349 according to the MK test.

350 The spatial distribution of the annual ETo over the YRB is shown in Fig. 4.

351 (a). The high ETo values were mainly located in the northern region of the upper

352 basin. In these regions, the annual ETos were mostly greater than 1100 mm. The ETo

353 values in the southern part of the upper basin were relatively low. A large part of this

354 area had an annual ETo less than or equal to 900 mm. The ETo values were between

355 900 and 1000 mm in the center of the upper basin and western region of the middle

356 basin and between 1000 and 1100 mm in the eastern region of the middle basin and

357 lower basin.

358 The spatial distribution of the ETo trends is presented in Fig. 4(b). The ETo

359 increased in most areas of the upper and middle basins and showed decreasing trends

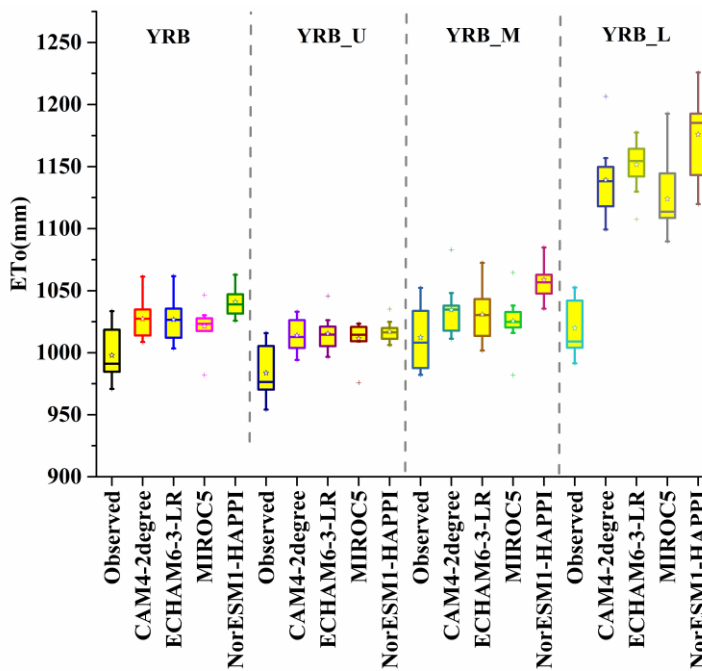
360 throughout the lower basin, the eastern and some northern parts of the middle basin

361 and the northeastern part of the upper basin. There were significant increasing trends

362 ($p < 0.05$) across wide areas in some of the central and southern parts of the upper

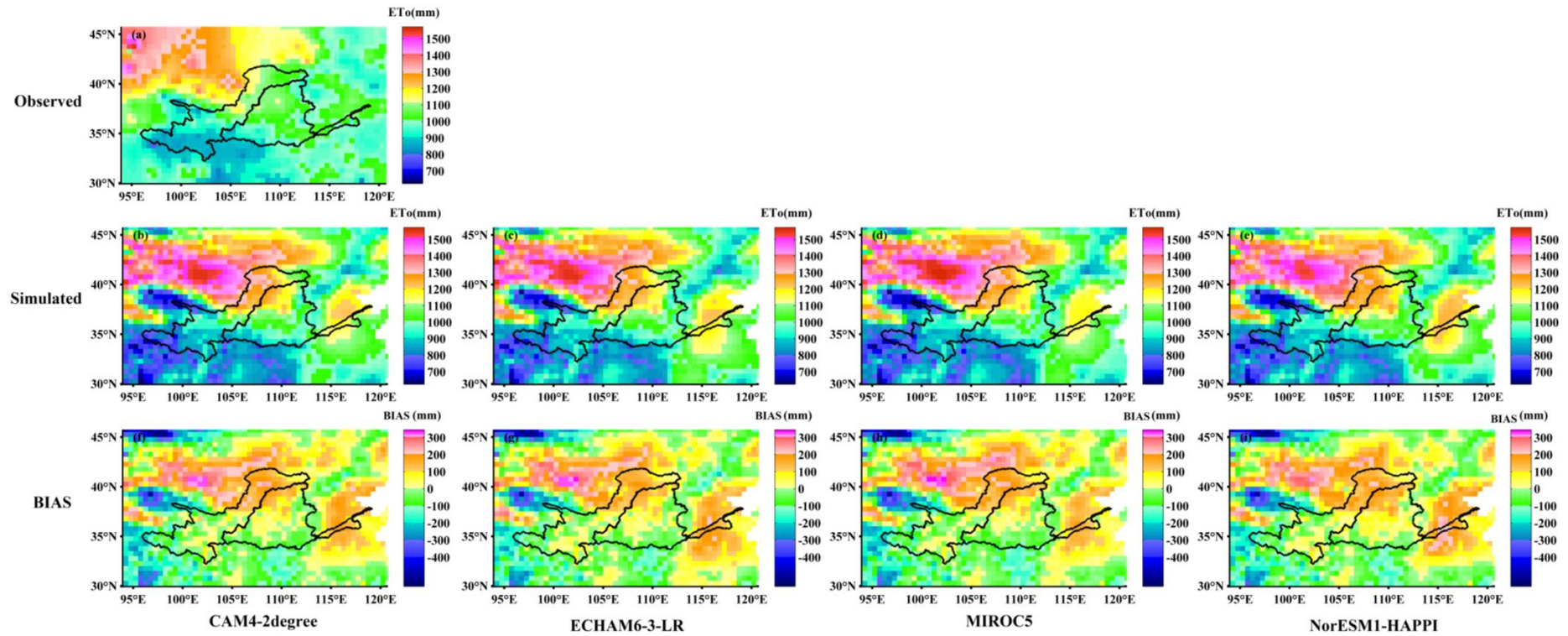
363 basin and the western part of the middle basin, where the ETo increased at over 0.5
 364 mm yr⁻¹. The ETo decreased significantly (p<0.05) in a fraction of the northeastern
 365 part of the upper basin, southeastern part of the middle basin and most of the lower
 366 basin, where the reduction rate exceeded 0.5 mm yr⁻¹. It can be seen from the plot that
 367 the ETo decreased most obviously in the lower basin, where the decreasing rate was
 368 over 1.5 mm yr⁻¹.

369 3.3 Evaluation of HAPPI simulations



370
 371 Fig. 5. Comparison of ETo calculated by observed data with ensemble mean ETo of mode
 372 calculated by HAPPI in the whole (YRB), upper (YRB_U), middle (YRB_M) and lower (YRB_L)
 373 basins during the reference period from 2006 to 2015. Horizontal lines in each boxplot represent
 374 the 10 years' 1st and 25th percentiles, median, and 75th and 99th percentiles, respectively; the star
 375 represents the mean ETo, and the plus signs represent the minimum and maximum.

376 The boxplots of the annual ETo based on the observations and simulations
377 from 2006 to 2015 in the whole, upper, middle and lower basins are shown in Fig. 5.
378 HAPPI has slightly higher simulation values for the ETo for the majority of the basin.
379 They give the best simulations of the ETo in the middle and upper basins and
380 relatively poor simulation in the lower basin. The biases of the multiyear average ETo
381 from the CAM4-2degree, ECHAM6-3-LR, MIROC5, and NorESM1-HAPPI were
382 29.4, 28.9, 23.6 and 43.2 mm for the whole basin, respectively, 30.5, 31.9, 28.0 and
383 33.4 mm for the upper basin, respectively, 22.2, 18.6, 13.3 and 46.4 mm for the
384 middle basin, respectively, and 119.2, 131.7, 104.0 and 156.1 mm for the lower basin,
385 respectively. Although the GCMs give the maximal bias for the ETo in the lower
386 basin, the lower basin is a very small part of the whole.



387

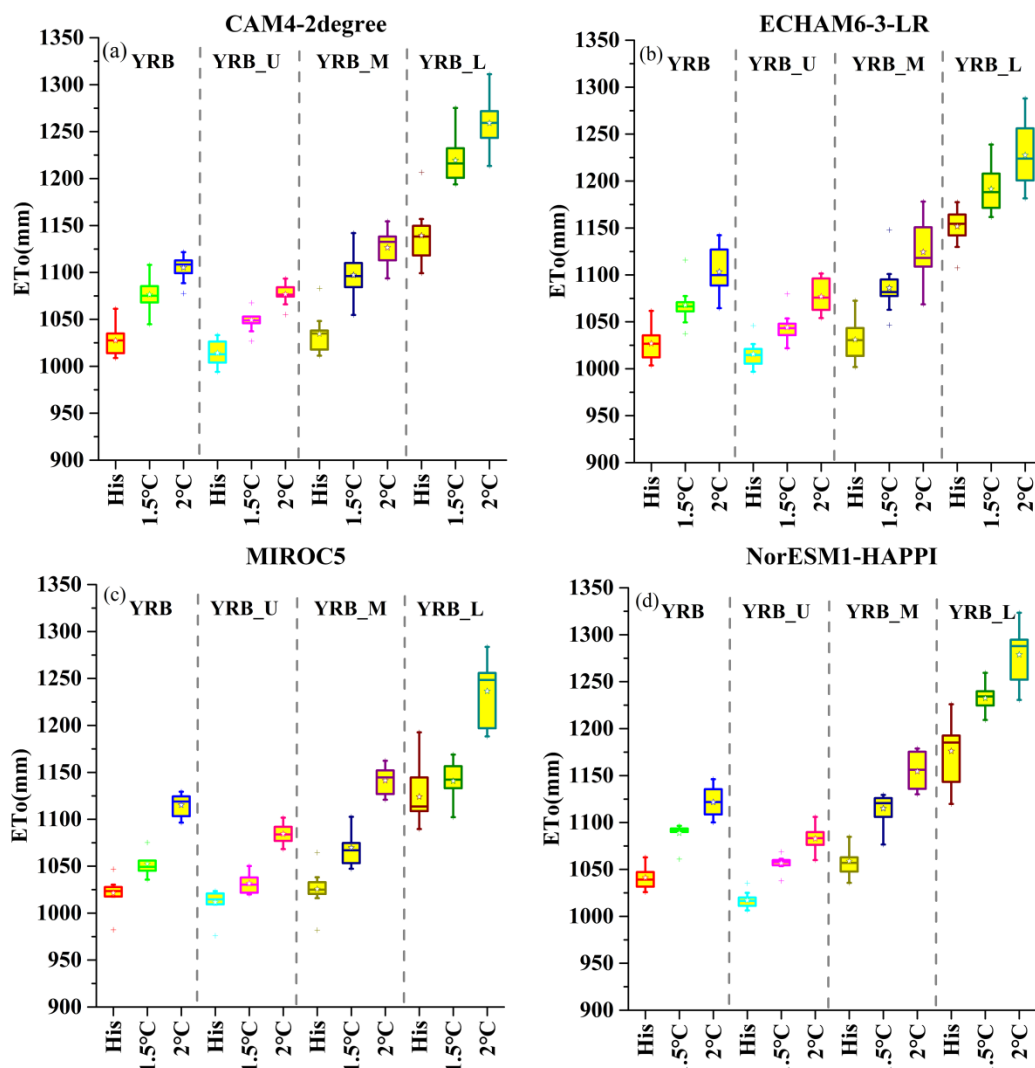
388 Fig. 6. Spatial patterns of the ETo estimated from: (a) observed and simulated data of (b) CAM4-2degree, (c) ECHAM6-3-LR, (d) MIROC5 and (e) NorESM1-

389 HAPPI and the difference between EToS calculated using simulated data of (f) CAM4-2degree, (g) ECHAM6-3-LR, (h) MIROC5 and (i) NorESM1-HAPPI and ETo

390 calculated using observed data during the period of 2006-2015. The simulated ETo were ensemble mean ETo of mode.

391 The spatial patterns of ETos estimated from observed and simulated data during 2006-
392 2015 are presented in Fig. 6 and were well simulated in the YRB. The spatial
393 distributions of the ETo from CAM4-2degree, ECHAM6-3-LR, MIROC5, and
394 NorESM1-HAPPI were similar to those of the ETo from observations, in which the
395 ETo was highest in the northern part of the upper basin, followed by the northwestern
396 part of the middle basin and the lower basin, the center of the middle basin, the
397 southern part of the middle basin and the center part of the upper basin. The ETos in
398 the southern part and west corner of the upper basin were also the lowest. The
399 correlation coefficients between the ETos calculated from observed data and from
400 CAM4-2degree, ECHAM6-3-LR, MIROC5, and NorESM1-HAPPI were 0.89, 0.89,
401 0.88 and 0.89, respectively, which is significant at the 99% confidence level.
402 However, HAPPI simulated higher ETos in the northern parts of both the upper and
403 middle basins and the lower basin, while a lower simulated ETo was obtained in some
404 southwestern parts of the upper basin and some southern parts of the middle basin.

3.4 ETo for global warming of 1.5 and 2.0 °C



406

407 Fig. 7. Comparison of ensemble mean ETo of mode in the whole (YRB), upper (YRB_U), middle
 408 (YRB_M) and lower (YRB_L) basins during the reference period from 2006 to 2015 and for the
 409 1.5 and 2.0 °C for (a) CAM4-2degree, (b) ECHAM6-3-LR, (c) MIROC5, (d) NorESM1-HAPPI.

410

The boxplots of the ETo in the reference period and for the 1.5 and 2.0 °C

411

increases over pre-industrial levels are shown in Fig. 7. The ETo is projected to

412

increase at both the 1.5 and 2°C global warming levels compared to the period of

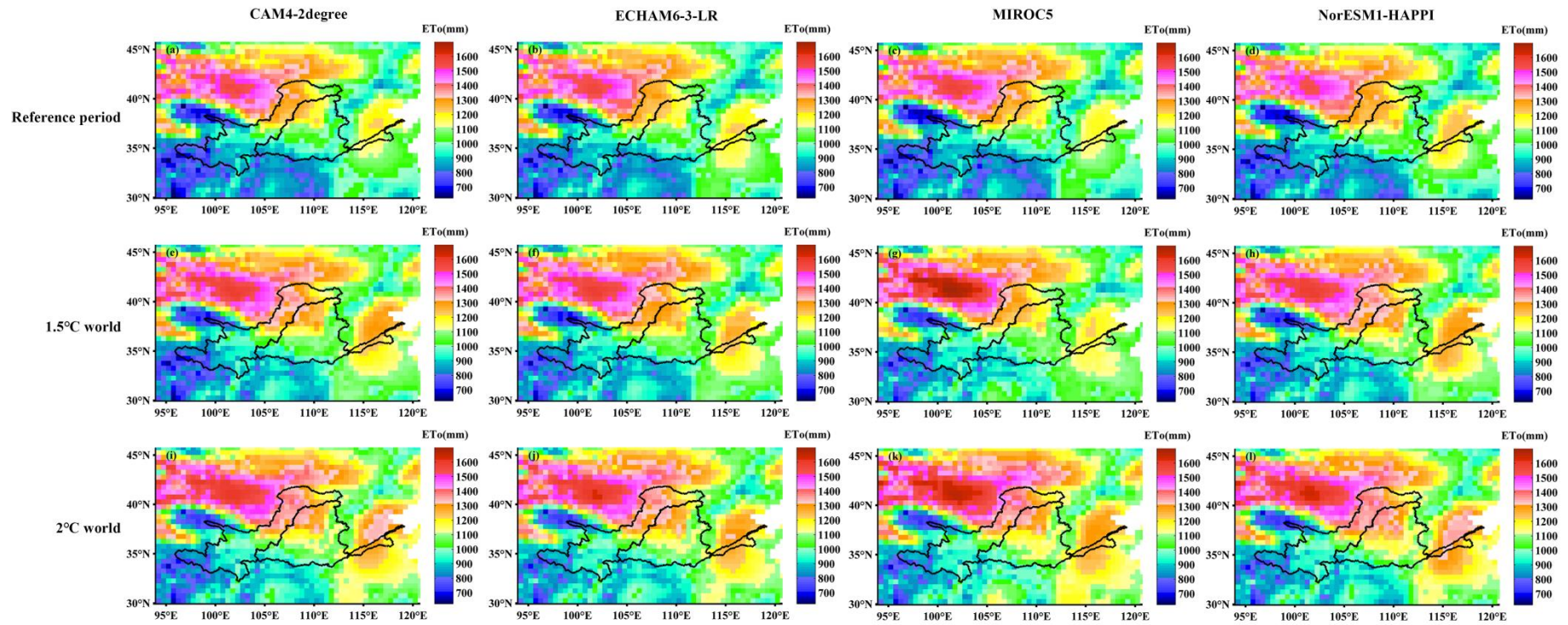
413

2005-2015 for each GCM. The increment of the ETo at the 2°C level is more than that

414 at the 1.5°C level. The ETo increases the most in the lower basin at both warming
415 levels. At the 1.5°C warming level, the multiyear average ETo increases by 49.1,
416 41.0, 30.9 and 47.6 mm in the whole basin for CAM4-2degree, ECHAM6-3-LR,
417 MIROC5 and NorESM1-HAPPI, respectively, compared to the reference period. The
418 increment of the multiyear average ETo in the upper basin is less than that in the
419 whole basin, and it reaches 35.1, 28.4, 20.0 and 39.4 mm for CAM4-2degree,
420 ECHAM6-3-LR, MIROC5 and NorESM1-HAPPI, respectively. The increments of
421 ETo for the CAM4-2degree, ECHAM6-3-LR, MIROC5 and NorESM1-HAPPI are
422 approximately 62.7, 55.1, 44.1, and 56.2 mm for the middle basin, respectively, and
423 80.2, 39.8, 16.8 and 56.4 mm for the lower basin. In the 2°C warming, the multiyear
424 average ETo for the CAM4-2degree, ECHAM6-3-LR, MIROC5 and NorESM1-
425 HAPPI increases by 77.9, 76.6, 93.7 and 80.6 mm for the whole basin, respectively,
426 62.7, 61.5, 72.8 and 65.8 mm for the upper basin, respectively, 91.9, 93.5, 115.7 and
427 95.7 mm for the middle basin, respectively, and 119.8, 75.8, 112.5 and 102.7 mm for
428 the lower basin, respectively.

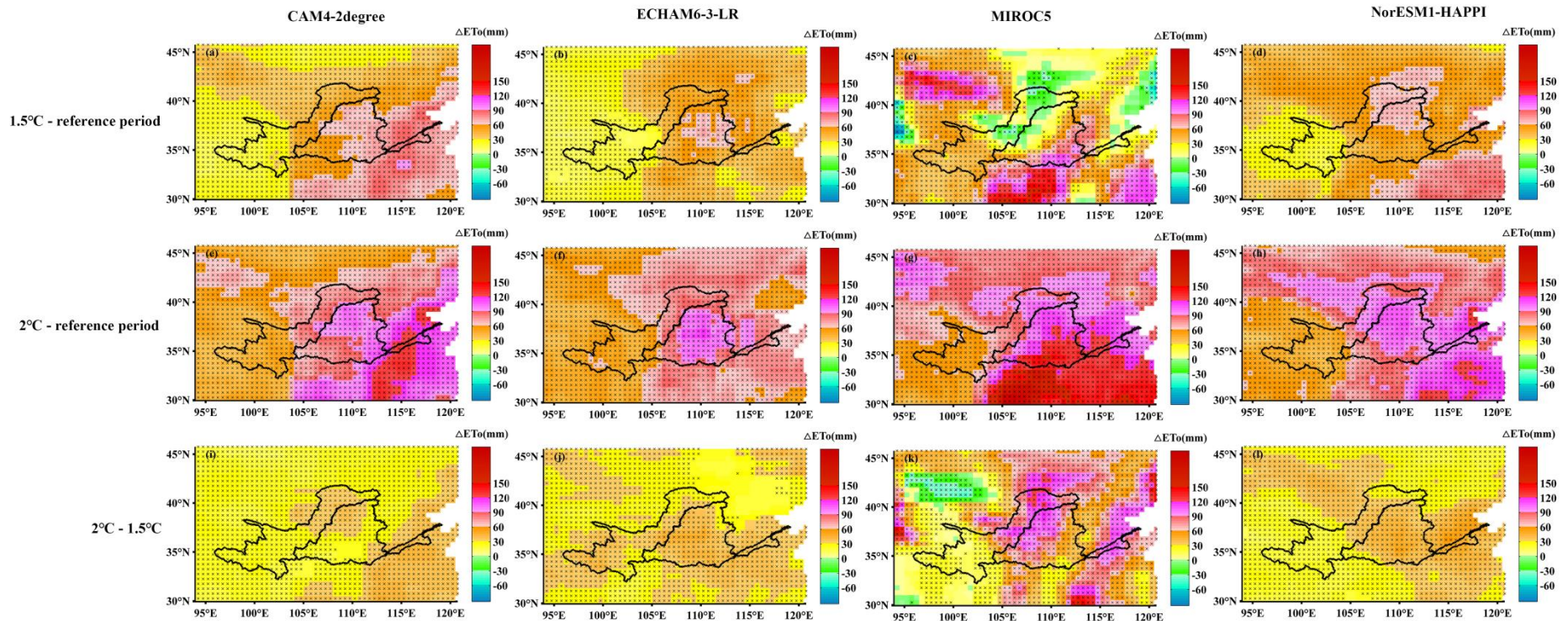
429 Compared to a 1.5°C warmer world, the ETo increases most obviously in the
430 lower basin in the 2°C warmer world. The increment increases to 28.7, 35.6, 62.8 and
431 33.0 mm in the whole basin for CAM4-2degree, ECHAM6-3-LR, MIROC5 and
432 NorESM1-HAPPI, respectively, implying that increases in the ETo of approximately
433 28.7-62.8 mm can be avoided by limiting global warming to 1.5°C. The ETo
434 projected by CAM4-2degree, ECHAM6-3-LR, MIROC5 and NorESM1-HAPPI
435 increases by 27.6, 33.1, 52.9 and 26.3 mm in the upper basin, respectively, 29.3, 38.4,

436 71.7 and 39.5 mm in the middle basin, and 39.6, 36.0, 95.7 and 46.3 mm in the lower
437 basin, respectively.



438 Fig. 8. Spatial distribution of ensemble mean ETo of mode at the reference period 1986 to 2005 (a, b, c, d) and at the 1.5°C (e, f, g, h) and 2°C warming levels (i, j,
 439 k, l). The 1st, 2nd, 3rd, and 4th columns denotes ETo calculated by CAM4-2degree (a, e, i), ECHAM6-3-LR (b, f, j), MIROC5 (c, g, k) and NorESM1-HAPPI (d, h,
 440 l), respectively.

441



442

443 Fig. 9. Spatial distribution of changes in ensemble mean ETo of mode at the 1.5°C (a, b, c, d) and 2.0°C warming levels (e, f, g, h) with respect to the
 444 period of 2006-2015 and the difference in ETo between the 2 and 1.5°C warming levels (i, j, k, l). Hatchings are statistically significant at the 5% level according to a
 445 two-sided t test (95% confidence). The 1st, 2nd, 3rd, and 4th columns denote ETo calculated by CAM4-2degree (a, e, i), ECHAM6-3-LR (b, f, j), MIROC5 (c, g, k)
 446 and NorESM1-HAPPI (d, h, l), respectively.

447 The spatial distributions of the ETo for the reference period 2006 to 2015 and
448 the 1.5 and 2.0°C warmer worlds are depicted in Fig. 8. Generally, the spatial patterns
449 of the ETo among the four GCMs of HAPPI show similar characteristics in the 1.5
450 and 2°C warmer worlds to the reference period; however, the changes in the ETo in
451 the different warming levels exhibit different spatial distributions among the different
452 GCMs (Fig. 9). Generally, the ETo increases significantly in almost the whole YRB at
453 the 1.5 and 2°C warming levels relative to the reference period for HAPPI.
454 Specifically speaking, at a global warming of 1.5°C, the ETo increases most in the
455 eastern region of the middle basin and lower basin for CAM4-2degree (>60 mm), the
456 center of the middle basin for ECHAM6-3-LR (>60 mm), the southeastern region of
457 the middle basin for MIROC5 (>60 mm) and northern parts of the upper and middle
458 basins for NorESM1-HAPPI (>60 mm). The changes in ETo are relatively small in
459 the upper basin for CAM4-2degree, ECHAM6-3-LR and NorESM1-HAPPI (<30
460 mm). For the MIROC5, the increment will be relatively small in the center of the
461 upper basin and the western region of the middle basin (<30 mm), and the ETo even
462 decreases in some areas of those regions.

463 For a 2°C warming world, the increment in the ETo is greater than 30 mm
464 relative to the reference period. The spatial patterns of the increment of the ETo at the
465 2°C warming level with respect to the reference period are similar to those at 1.5°C,
466 but the increment is greater and the ETo increases by more than 90 mm in most of the
467 middle basin and lower basin for all GCMs.

468 The ETo increases significantly at the 2°C warming level compared to that at
469 1.5°C. There is a large increment in the ETo in the northern portion of the upper and
470 middle basins and the lower basin, with an increment over 30 mm for
471 CAM4-2degree and over 60 mm for MIROC5. The ETo increases by more than 30
472 mm in almost the whole basin for ECHAM6-3-LR and in the center of the upper basin
473 and almost the whole middle and lower basins for NorESM1-HAPPI. Although the
474 changes in the ETo between the two warming levels are diverse among GCMs, there
475 is good consistency in that they are largest in the middle-northern area of the upper
476 basin (southern part of Hetao Plain), the northwest of the middle basin (Ordos Plateau
477 and northwest part of the Loess Plateau) and the lower basin (North China Plain).

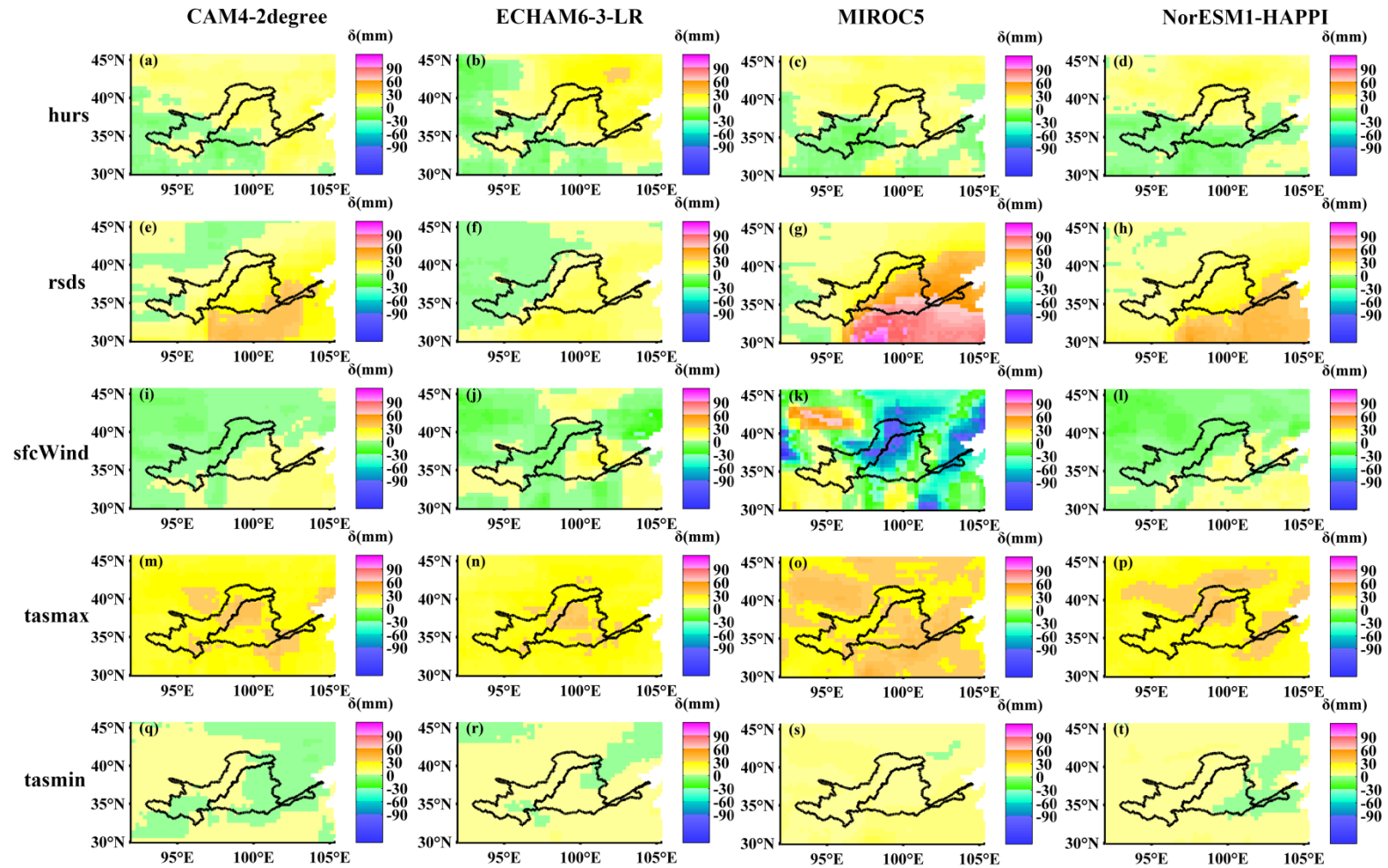
478 3.5 Contribution of climatic variables to ETo change

479 The areal average of the contribution from a climatic variable to the change in
480 the ETo for the whole, upper, middle and lower basins is listed in Tab. 3. The sum of
481 the contributions from a single climatic variable to the ETo is unequal to the
482 contribution from all variables (increment of ETo), but there is little difference
483 between the two in most cases. The simple method was adopted to determine the
484 relative contributions of the variables to the change of ETo. Broadly, the tasmax gives
485 most positive contribution to the increase of ETo in the YRB at the 1.5 and 2°C
486 warming levels, which is revealed by almost all GCMs. rsds also gives a certain
487 positive contribution to the increase of the ETo at the two warming levels. An
488 exception is that the main reason for the increase of the ETo projected by MIROC5 at

489 1.5°C warming is the rsds for the whole, middle and lower basins and the tmax for the
 490 upper basin. Hurs gives some positive contribution to ETo projected by ECHAM6-3-
 491 LR, which is greater than rsds at both warming levels. Specially, sfsWind has a great
 492 negative effect on the increase of ETo at the 1.5°C warming level for MIROC5. All in
 493 all, sfsWind and tmin make little contributions to the increase in ETo under global
 494 warming of 1.5 and 2°C.

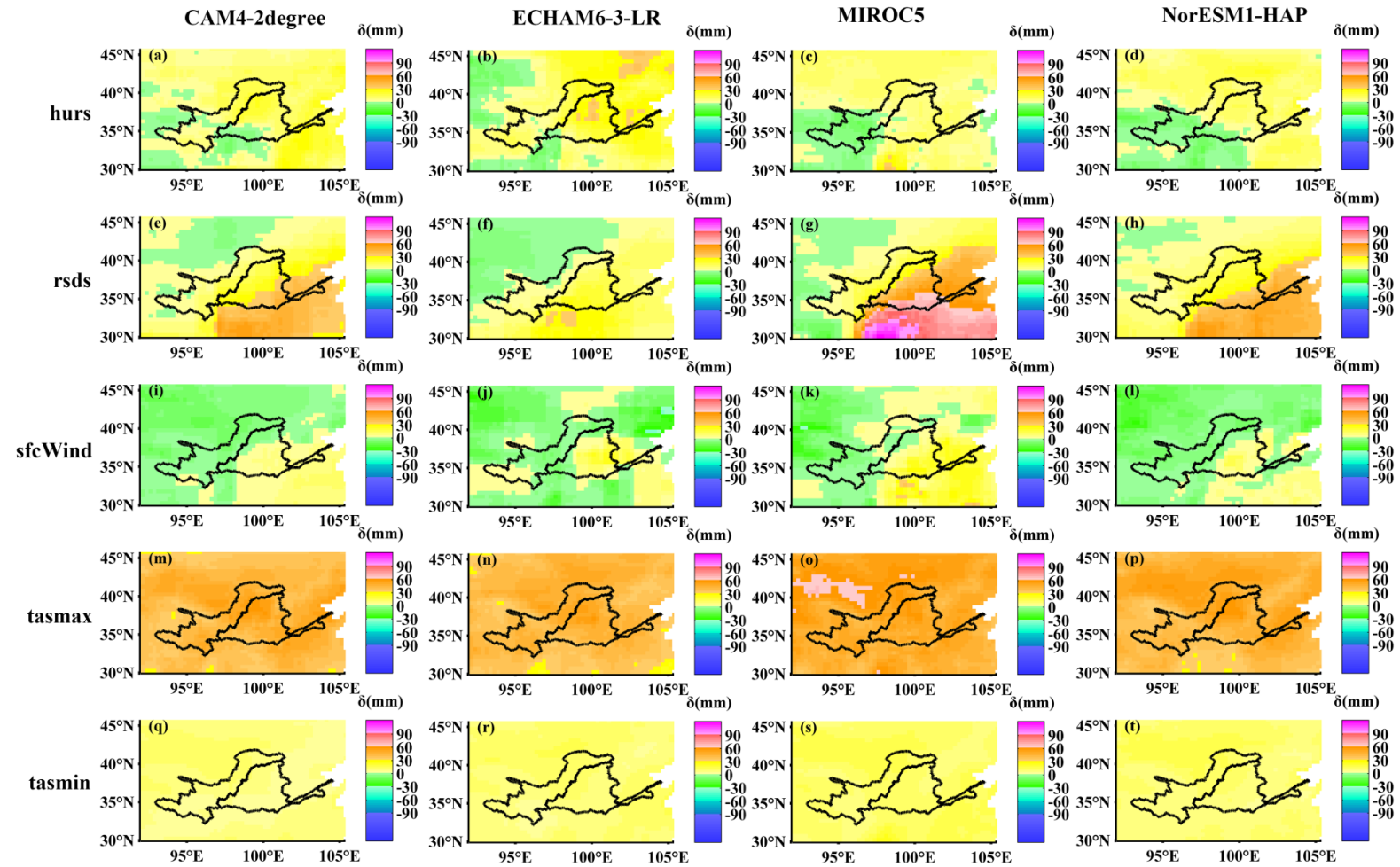
495 Tab. 3. Contributions of climatic variable to changes in ETo at 1.5 and 2°C warming levels

| 496 | CAM4-2degree | | | | ECHAM6-3-LR | | | | MIROC5 | | | | NorESM1-HAPPI | | | | |
|-------------------------|-------------------------|-------|-------|-------|-------------|-------|-------|-------|--------|-------|-------|-------|---------------|-------|-------|-------|-------|
| | YRB | YRB_U | YRB_M | YRB_L | YRB | YRB_U | YRB_M | YRB_L | YRB | YRB_U | YRB_M | YRB_L | YRB | YRB_U | YRB_M | YRB_L | |
| Global warming of 1.5°C | hurs | 5.6 | 4.4 | 6.4 | 12.2 | 10.2 | 7.4 | 12.9 | 16.3 | 2.3 | 1.2 | 3.3 | 3.9 | 1.8 | 3 | 0.7 | -1.9 |
| | rsds | 16.2 | 8.3 | 23.9 | 34 | 7.1 | 1.8 | 12.9 | 8.5 | 33.4 | 15.6 | 51.7 | 57.6 | 16.2 | 9.7 | 22.1 | 36.2 |
| | sfsWind | 0.9 | -1.4 | 3 | 7.5 | 2.2 | -0.8 | 5.4 | 4.4 | -39.5 | -32.3 | -45.7 | -64.7 | -1 | -3.5 | 1.5 | 3.2 |
| | tmax | 30.2 | 28.6 | 32 | 30.8 | 29.5 | 27.4 | 31.9 | 29.1 | 31.9 | 30.3 | 33.6 | 33.3 | 29.9 | 29.1 | 30.6 | 32.7 |
| | tmin | 1.7 | 2.3 | 2.3 | 0.1 | 3.1 | 3.3 | 3.3 | 4.6 | 5.1 | 5 | 5 | 7.3 | 3.3 | 4.1 | 4.1 | 0.6 |
| | sum | 54.7 | 42.2 | 67.7 | 84.6 | 52.1 | 39 | 66.4 | 62.8 | 33.2 | 19.9 | 47.8 | 37.4 | 50.1 | 42.4 | 59 | 70.8 |
| | Increment of ETo | 49.1 | 35.1 | 62.7 | 80.2 | 41.0 | 28.4 | 55.1 | 39.8 | 30.9 | 20.0 | 44.1 | 16.8 | 47.6 | 39.4 | 56.2 | 56.4 |
| Global warming of 2°C | hurs | 10.3 | 9.2 | 10.9 | 20.3 | 17.7 | 13 | 22.5 | 25.5 | 4 | 0.6 | 7.6 | 6.6 | 5.2 | 3.3 | 6.9 | 9.2 |
| | rsds | 18.3 | 8.9 | 27.4 | 39.7 | 10.5 | 4.4 | 17.3 | 11.7 | 30.6 | 13.3 | 48.3 | 53.5 | 20.3 | 11.2 | 28.6 | 45.9 |
| | sfsWind | 0.2 | -2.6 | 2.7 | 8.4 | 3.1 | -0.8 | 7.3 | 5.1 | 5.4 | -0.4 | 10.8 | 22.7 | -0.1 | -3.4 | 3.5 | 1.9 |
| | tmax | 46.5 | 44.8 | 48 | 52 | 45.9 | 44.9 | 47.1 | 43.7 | 50.9 | 50.6 | 51.3 | 49.4 | 46.7 | 45.5 | 47.7 | 52.6 |
| | tmin | 7.0 | 7.9 | 7.9 | 5.4 | 9.7 | 9.6 | 9.6 | 12.7 | 12 | 12.1 | 12.1 | 14.6 | 9.8 | 10.3 | 10.3 | 7.5 |
| | sum | 82.3 | 68.2 | 96.8 | 125.8 | 86.9 | 71.1 | 103.8 | 98.6 | 102.9 | 76.2 | 130.1 | 146.8 | 81.9 | 66.9 | 97.1 | 117.1 |
| | Increment of ETo | 79.9 | 62.7 | 91.9 | 119.8 | 76.6 | 61.5 | 93.5 | 75.8 | 93.7 | 72.8 | 115.7 | 112.5 | 80.6 | 65.8 | 95.7 | 102.7 |



498 Fig. 10. Spatial distribution of the contributions to the ETo change at the 1.5°C warming level. The 1st, 2nd, 3rd, 4th, and 5th rows indicates contributions of hurs (a,
499 b, c, d), rsds (e, f, g, h), sfcWind (i, j, k, l), tmax (m, n, o, p), and tmin (q, r, s, t), respectively. The 1st, 2nd, 3rd, and 4th columns denote contributions for CAM4-
500 2degree (a, e, i, m, q), ECHAM6-3-LR (b, f, j, n, r), MIROC5 (c, g, k, o, s) and NorESM1-HAPPI (d, h, l, p, t), respectively.

501 The spatial distributions of the contribution from a climatic variable to the
502 change of the ETo at global warming of 1.5 and 2°C are shown in Fig. 10 and
503 Fig. 11, respectively. At the 1.5°C warming level, the change in hurs has a negative
504 effect on ETo at the southern part of the YRB and a positive effect at the northern part
505 of the YRB. The change of rsds leads to an increase in the ETo in the whole basin for
506 4GCMs, except that it causes a decrease in ETo at the southern part of the upper basin
507 for ECHAM6-3-LR. The change of sfcWind has a positive contribution to ETo in
508 most of the middle and lower basins for CAM4-2degree, ECHAM6-3-LR and
509 NorESM1-HAPPI. It induces an increase in ETo only at the southern portion of the
510 upper basin for MIROC5. The tasmax gives a different level of increase in the ETo in
511 the whole basin for all GCMs. The change of the tasmin has a positive contribution to
512 the increase in ETo in most of the area of the YRB projected by HAPPI. It gives a
513 negative contribution to ETo in the southern portion of the upper basin, eastern part of
514 the middle basin and the lower basin for CAM4-2degree and at the eastern corner of
515 the middle basin and the lower basin for NorESM1-HAPPI.



516

517

Fig. 11. As in Fig. 10, but for the 2°C warming level.

518 At the 2°C warming level, the contribution of the climatic variables has good
 519 consistency among the GCMs of HAPPI. The change of the hurs causes an increase of
 520 the ETo in the whole YRB for CAM4-2degree and ECHAM6-3-LR, and it gives rise
 521 to a decrease of ETo in the southern region of the upper basin and an increase of the
 522 ETo in the northern part of the upper basin and in the middle and lower basins for
 523 MIROC5 and NorESM1-HAPPI. The changes of the rds, tasmax and tasmin make a
 524 positive contribution to the ETo in the entire YRB for all GCMs. The sfcWind still
 525 gives a negative contribution to the decrease of the ETo in the upper basin and
 526 western edge of the middle basin for all GCMs, and it gives a positive contribution at
 527 the central and eastern portions of the middle basin. It induces an increase in the ETo
 528 at the lower basin for CAM4-2degree, ECHAM6-3-LR and MIROC5 and a decrease
 529 of ETo for NorESM1-HAPPI.

530 **4 Discussions**

531 Tab. 4. Warming levels in the YRB during the 1.5 and 2.0 °C global warming above the pre-
 532 industrial level.

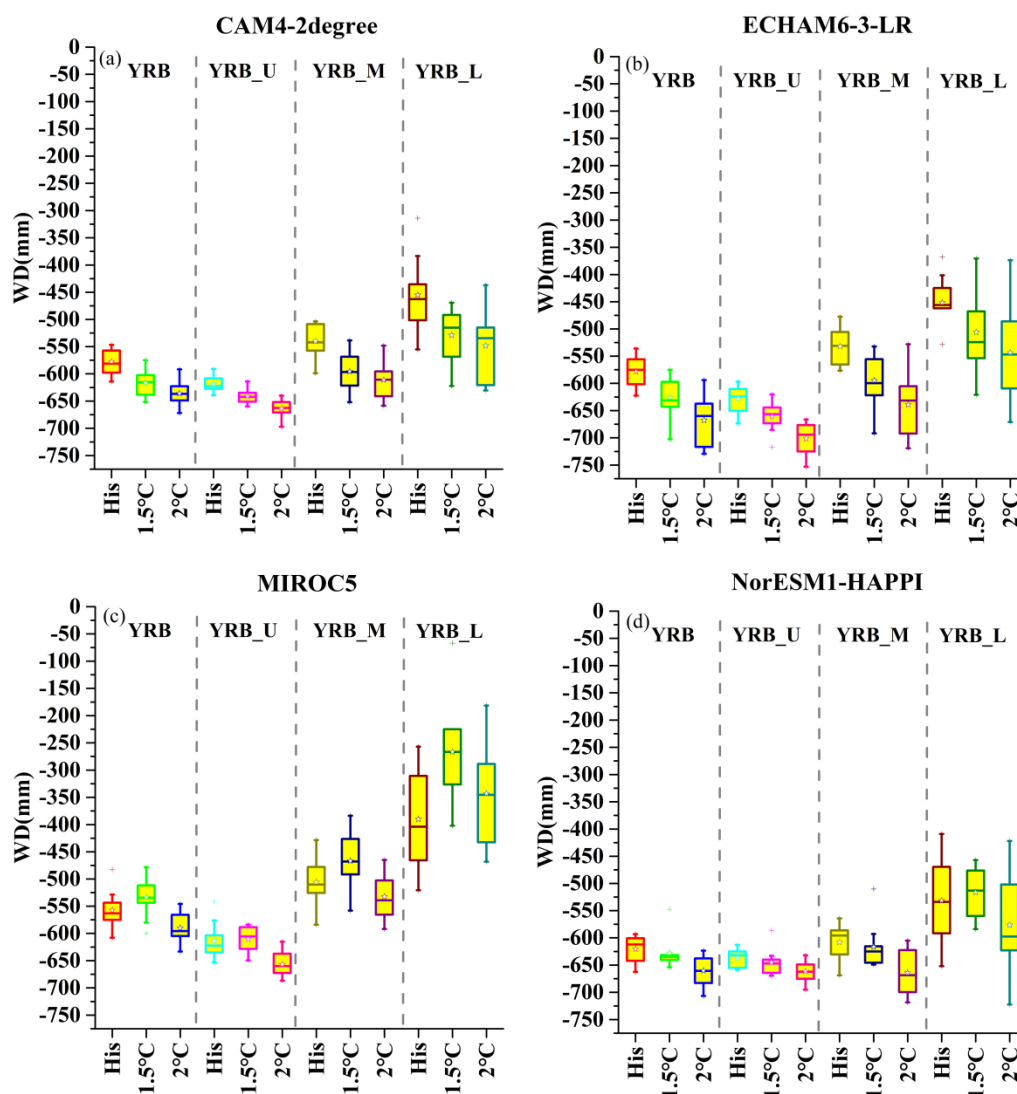
| | Global warming of 1.5°C | | | | Global warming of 2°C | | | |
|-------|-------------------------|-------------|--------|---------------|-----------------------|-------------|--------|---------------|
| | CAM4-2degree | ECHAM6-3-LR | MIROC5 | NorESM1-HAPPI | CAM4-2degree | ECHAM6-3-LR | MIROC5 | NorESM1-HAPPI |
| YRB | 1.62 | 1.66 | 1.98 | 1.79 | 2.27 | 2.33 | 2.64 | 2.51 |
| YRB_U | 1.57 | 1.64 | 1.92 | 1.77 | 2.25 | 2.32 | 2.65 | 2.49 |
| YRB_M | 1.67 | 1.69 | 2.06 | 1.81 | 2.3 | 2.34 | 2.65 | 2.54 |
| YRB_L | 1.65 | 1.58 | 1.96 | 1.65 | 2.26 | 2.23 | 2.43 | 2.31 |

534 Tab. 5. Changes of the precipitation in the YRB during the 1.5 and 2.0 °C global warming
 535 compared to the reference period.

| | Global warming of 1.5°C | | | | Global warming of 2°C | | | |
|-------|-------------------------|-------------|--------|---------------|-----------------------|-------------|--------|---------------|
| | CAM4-2degree | ECHAM6-3-LR | MIROC5 | NorESM1-HAPPI | CAM4-2degree | ECHAM6-3-LR | MIROC5 | NorESM1-HAPPI |
| YRB | 9.98 | -6.28 | 54.51 | 39.99 | 19.45 | -12.59 | 61.12 | 40.81 |
| YRB_U | 12.55 | -4.78 | 23.3 | 31.19 | 17.61 | -11.8 | 29.91 | 41.08 |
| YRB_M | 7.35 | -7.4 | 83.5 | 47.66 | 21.01 | -13.24 | 89.26 | 39.37 |
| YRB_L | 6.48 | -14.64 | 140.23 | 71.65 | 26.61 | -16.03 | 159.6 | 57.71 |

536 Changes of the mean temperature compared to the pre-industrial level and
 537 changes of the precipitation compared to the reference period at the 1.5 and 2.0 °C
 538 global warming in the YRB are listed in Tab. 4 and 5, respectively. The global mean
 539 surface temperature for the period of 2006–2015 was 0.87°C higher than the average
 540 over the 1850–1900 period (IPCC, 2018). The warming above the pre-industrial level
 541 in the YRB during the 1.5 and 2.0 °C global warming levels is the increment of the
 542 mean temperature at the 1.5 and 2.0°C warming relative to the reference period plus
 543 0.87°C, respectively. At the 1.5 and 2°C warmings, the whole YRB is warmer than
 544 during pre-industrial times, particularly for the middle basin, where the warming level
 545 is higher than in the other regions. The precipitation shows increasing trends for
 546 CAM4-2degree, MIROC5, NorESM1-HAPPI in a 1.5 and 2°C warming world
 547 compared to the reference period. The precipitation values at 2°C warming are greater
 548 than at 1.5°C warming for CAM4-2degree and MIROC5. The precipitation projected
 549 by NorESM1-HAPPI at the 2°C warming level is higher for the whole and upper
 550 basins and lower for the middle and lower basins than at the 1.5°C warming level.
 551 The precipitation projected by ECHAM6-3-LR both at 1.5 and 2°C warming shows

552 decreasing trends, and it decreases more at 2°C warming than at 1.5°C warming. All
 553 in all, given the increase of the air temperature and precipitation, we are interested in
 554 whether YRB will have dry or wet conditions.

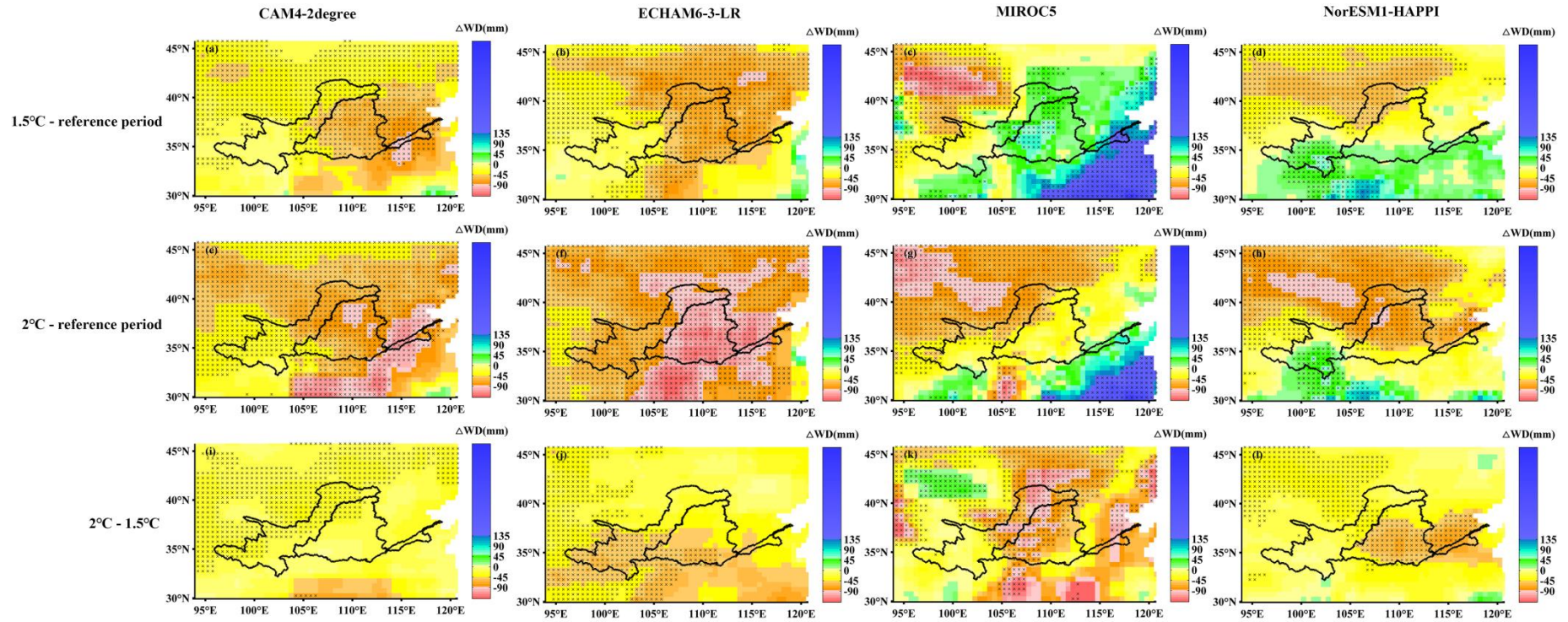


555
 556 Fig. 12. Comparison of ensemble mean WD of mode in the whole (YRB), upper (YRB_U), middle
 557 (YRB_M) and lower (YRB_L) basins during the reference period from 2006 to 2015 and under
 558 global warming of 1.5°C and 2.0°C for (a) CAM4-2degree, (b) ECHAM6-3-LR, (c) MIROC5, (d)
 559 NorESM1-HAPPI.

560 The climatic water deficit (WD, difference between the precipitation and ETo)
561 is calculated for the reference period and the 1.5 and 2°C global warming level. It can
562 be seen as an aridity index that can accurately quantify the water supply needed for a
563 reference crop (Paltineanu et al., 2007, 2009). It provides a simple measure of the
564 water surplus or deficit (Vicente-Serrano, Sergio et al., 2010). Boxplots of the annual
565 WD for the whole, upper, middle and lower basins are presented in Fig. 12. Except for
566 MIROC5, the WD under the three GCMs show decreasing trends at two warming
567 levels compared to the reference period. At 2°C warming, the WDs projected by all
568 four GCMs generally have more serious decreases in the whole basin. Generally, WD
569 has a greater decrease in the middle and lower basins. The WD presents an increasing
570 trend for MIROC5 at the 1.5°C warming level due to the projected increase in
571 precipitation; however, it decreases with the additional 0.5°C warming. As a
572 consequence, the YRB may experience drier conditions in a warmer world, and it is
573 more serious at the 2°C warming level.

574

575



576

577

Fig. 13. As in Fig. 9, but for WD.

578 Fig. 13 shows the *changes* of the spatial patterns instead of the *absolute* spatial patterns
579 of WD at different periods and shows that a majority of the YRB is characterized by decreasing
580 trends in the WD at two warming levels projected by HAPPI, except for MIROC5. The WD
581 decreases more in the 2°C warmer world in the entire basin by all GCMs of HAPPI. The
582 increment of the ETo exceeds the increment of the precipitation, causing drier conditions in most
583 area of YRB. On account of the great increase in precipitation at 1.5°C warming in the middle
584 and lower basins projected by MIROC5 and in the south of YRB projected by NorESM1-
585 HAPPI, these regions become wetter. The spatial patterns of change in WD are varied from
586 GCMs, however, all GCMs give a consistent result that an additional 0.5°C warming will make
587 almost the whole YRB drier.

588 Some researchers have analyzed the impact factors of the ETo in the YRB during the
589 observed period by the contribution estimation method or sensitivity analysis method and found
590 that the impact factors of changing in ETo varied spatially. Liu et al., (2010) revealed that there
591 was a high sensitivity coefficient for ETo from 1961 to 2006 for the solar radiation for the upper
592 basin, the wind speed for the northwest portion of the middle basin, relative humidity for the
593 south portion of YRB and air temperature for the west portion of the upper basin and the north
594 portion of the middle basin. Wang et al., (2012) discovered that the dominant factor for the
595 decline in the ETo during 1957-2008 was a decrease in the wind speed in the west and north of
596 the Loess Plateau and reduced sunshine duration in the middle-lower Yellow River Plain, while
597 the dominant factor for the increase of ETo was an increasing mean temperature in the source
598 area of the YRB. Our results revealed that the *tasmax* and *rsds* are the major driving forces for
599 the increase of ETo at the 1.5 and 2°C warming levels and that the impact factors have good
600 spatial consistency. It is likely that our results are different from the historical period because of

601 the changes in the climatic environment. The impact factor of ETo may change in a warmer
602 world, and the dominant factor is the maximum temperature. Contrary to the “evaporate
603 paradox”, ETo does not show a decreasing trend with the climate warming, it increases
604 significantly, which may change the climatic environment of the YRB.

605 Our findings are supported by previous studies. Li et al. (2012) found that HadCM3
606 projects a continuous increase of ETo during the 21st century on the Loess Plateau. ETo will
607 increase by approximately 4%, 7% and 12% for the three periods 2011-2040, 2041-2070 and
608 2071-2099, respectively. Su et al. (2018) revealed that 13 global climate models (GCMs) in the
609 CMIP5 project significant increases in the ETo throughout China for both target periods.
610 Although the first above result does not consider 1.5 and 2°C warming, our consistent finding is
611 that the ETo might increase in the warmer world. A major limitation of this study is the
612 uncertainty of the results. In section 3.3, we evaluated HAPPI’s simulations of the multiyear
613 averaged ETo and spatial pattern of the ETo. Although the GCMs give a minor error on the areal
614 averaged ETo and prominent performance on the spatial distribution of the ETo, their
615 simulations are larger than the ETo estimated by observed data. They show a large bias over
616 100 mm in the lower basin, northern part of the upper basin and northwestern portion of the
617 middle basin. Downscaling methods can give a better simulation of realistic climate variables
618 (Zhang et al., 2016), and after bias correction and statistical disaggregation, the uncertainty can
619 be reduced with respect to the observation (Su et al., 2016). Moreover, some uncertainty might
620 arise from inter-GCMs of HAPPI. GCMs give a consistent increase of ETo under global
621 warming of 1.5 and 2°C, but the magnitude of the increase and its spatial pattern are diverse. It is
622 not easy to determine which GCM is better than others. We do not calculate ensemble

623 projections from multiple GCMs, which may smooth the differences among GCMs, preferring to
624 provide the true results for each GCM.

625 **5 Conclusions**

626 In this study, we investigated the spatiotemporal distribution of ETo in the YRB during
627 1961–2017 based on observed data and projected the ETo under global warming of 1.5 and 2°C
628 based on outputs from HAPPI. The relative contributions of the climatic variables to change in
629 ETo were quantified to determine the causes of the change in ETo at two warming levels. We
630 also discussed changes in the climatic water deficit (difference between the precipitation and
631 ETo) to assess wet/dry variations in the YRB in a warmer world. The following conclusions can
632 be drawn from this study:

633 The ETo and ETo-trends exhibited spatial heterogeneity due to the complex spatial
634 patterns during 1961-2017 in the YRB, and the ETo increased significantly for the upper basin
635 (0.5 mm yr^{-1}) and decreased significantly for the middle (-0.23 mm yr^{-1}) and lower (-1.04 mm yr^{-1})
636 basins. The ETo value was the highest in the northern region of the upper basin ($>1100 \text{ mm}$),
637 followed by the eastern region of the middle basin and the lower basin (1000-1100 mm), the
638 center of the upper basin and western region of the middle basin (900-1000 mm) and the
639 southern part of the upper basin ($<900 \text{ mm}$). Furthermore, the ETo increased significantly in the
640 central and southern portions of the upper basin and the western portion of the middle basin, and
641 it decreased significantly in a small part of the northeastern portion of the upper basin, the
642 eastern portion of the middle basin and the lower basin.

643 HAPPI gave excellent simulations of the annual averages of ETo and spatial patterns of
644 ETo in the reference period (2006-2015) in the YRB. There is a small bias for the higher ETo in

645 the northern portion of the upper and middle basins and the lower basin and a lower ETo in the
646 southwestern portion of the upper basin and southern portion of the middle basin.

647 The multiyear average ETo of the YRB projected by CAM4-2degree, ECHAM6-3-LR,
648 MIROC5 and NorESM1-HAPPI increases by 49.1, 41.0, 30.9 and 47.6 mm for a 1.5°C warmer
649 world, respectively, and 77.9, 76.6, 93.7 and 80.6 mm for a 2°C warmer world, respectively,
650 compared to compared to in the reference period. The ETo increases the most in the lower basin
651 at both warming levels, follow by middle and upper basins. The increment in the ETo exceeds
652 the increment of the precipitation in a warmer world and this may intensify the aridity of YRB.
653 Limiting global warming to 1.5°C is beneficial to YRB for the lesser ETo and aridity. HAPPI
654 gives a consistent projection that the ETo will decrease over 30mm in the lower basin (North
655 China Plain), middle-northern area of the upper basin (southern part of Hetao Plain) and
656 northwestern are of the middle basin (Ordos Plateau and northwestern part of the Loess Plateau)
657 by limiting global warming to 1.5°C.

658 In a warmer world, tasmax has the greatest effect on the increase of ETo, and the causes
659 of the increase in ETo at the 1.5 and 2°C warming levels have good spatial consistency. rsds and
660 hurs also have contributions to the increase in ETo. sfsWind and tasmin have smaller
661 contributions to the increase of ETo.

662 **Acknowledgments**

663 This study is jointly sponsored by the National Key R&D Program of China
664 (2016YFA0600404), the National Natural Science Foundation of China (41530532), the China
665 Special Fund for Meteorological Research in the Public Interest (GYHY201106028), and the
666 Jiangsu Collaborative Innovation Center for Climate Change. We acknowledge the HAPPI core

667 team and NERSC for data storage. DMM was supported by a NERC independent research
668 fellowship (NW/N014057/1).

669 **Reference**

670 Allen, R. G., Pereira, L. S., Raes, D., & Smith, M. (1998). Crop evapotranspiration—Guidelines for computing
671 crop water requirements. FAO Irrigation and Drainage Paper 56, Rome, Italy. Retrieved from
672 https://appgeodb.nancy.inra.fr/biljou/pdf/Allen_FAO1998.pdf

673 Baker, H. S., Millar, R. J., Karoly, D. J., Beyerle, U., Guillod, B. P., Mitchell, D., et al. (2018). Higher CO₂
674 concentrations increase extreme event risk in a 1.5 °C world. *Nature Climate Change*, 8(7), 604-608.
675 <https://doi.org/10.1038/s41558-018-0190-1>

676 Bandyopadhyay, A., Bhadra, A., Raghuwanshi, N. S., & Singh, R. (2009). Temporal Trends in Estimates of
677 Reference Evapotranspiration over India. *Journal of Hydrologic Engineering*, 14(5), 508-515.
678 [https://doi.org/10.1061/\(ASCE\)HE.1943-5584.0000006](https://doi.org/10.1061/(ASCE)HE.1943-5584.0000006)

679 Burn, D. H., & Hesch, N. M. (2007). Trends in evaporation for the Canadian Prairies. *Journal of Hydrology*,
680 336(1), 61-73. <https://doi.org/10.1016/j.jhydrol.2006.12.011>

681 Cai, X., & Rosegrant, M. W. (2004). Optional water development strategies for the Yellow River Basin:
682 Balancing agricultural and ecological water demands. *Water Resources Research*, 40(8).
683 <https://doi.org/doi:10.1029/2003WR002488>

684 Chattopadhyay, N., & Hulme, M. (1997). Evaporation and potential evapotranspiration in India under
685 conditions of recent and future climate change. *Agricultural and Forest Meteorology*, 87(1), 55-73.
686 [https://doi.org/10.1016/S0168-1923\(97\)00006-3](https://doi.org/10.1016/S0168-1923(97)00006-3)

687 Cong, Z., Yang, D., Gao, B., Yang, H., & Hu, H. (2009). Hydrological trend analysis in the Yellow River
688 basin using a distributed hydrological model. *Water Resources Research*, 45(7).
689 <https://doi.org/doi:10.1029/2008WR006852>

690 Cuo, L., Zhang, Y., Gao, Y., Hao, Z., & Cairang, L. (2013). The impacts of climate change and land cover/use
691 transition on the hydrology in the upper Yellow River Basin, China. *Journal of Hydrology*, 502, 37-52.
692 <https://doi.org/10.1016/j.jhydrol.2013.08.003>

- 693 Döll, P., Trautmann, T., Gerten, D., Schmied, H. M., Ostberg, S., Saaed, F., & Schleussner, C.-F. (2018). Risks for
694 the global freshwater system at 1.5 °C and 2 °C global warming. *Environmental Research Letters*, 13(4),
695 044038. <https://doi.org/10.1088/1748-9326/aab792>
- 696 Douglas, I. (1989). Land degradation, soil conservation and the sediment load of the Yellow River, China:
697 Review and assessment. *Land Degradation & Development*, 1(2), 141-151.
698 <https://doi.org/doi:10.1002/ldr.3400010206>
- 699 Fu, G., Chen, S., Liu, C., & Shepard, D. (2004). Hydro-Climatic Trends of the Yellow River Basin for the Last
700 50 Years. *Climatic Change*, 65(1), 149-178. <https://doi.org/10.1023/B:CLIM.0000037491.95395.bb>
- 701 Golubev, V. S., Lawrimore, J. H., Groisman, P. Y., Speranskaya, N. A., Zhuravin, S. A., Menne, M. J., et al.
702 (2001). Evaporation changes over the contiguous United States and the former USSR: A reassessment.
703 *Geophysical Research Letters*, 28(13), 2665-2668. <https://doi.org/doi:10.1029/2000GL012851>
- 704 Gong, L., Xu, C.-y., Chen, D., Halldin, S., & Chen, Y. D. (2006). Sensitivity of the Penman–Monteith
705 reference evapotranspiration to key climatic variables in the Changjiang (Yangtze River) basin. *Journal of*
706 *Hydrology*, 329(3), 620-629. <https://doi.org/10.1016/j.jhydrol.2006.03.027>
- 707 Hobbins, M. T. (2004). Regional evapotranspiration and pan evaporation: Complementary interactions and
708 long-term trends across the Conterminous United States (Doctoral dissertation), Fort Collins, CO:
709 Colorado State University.
- 710 IPCC, 2018: *Summary for Policymakers. In: Global warming of 1.5°C. An IPCC Special Report on the*
711 *impacts of global warming of 1.5°C above pre-industrial levels and related global greenhouse gas*
712 *emission pathways, in the context of strengthening the global response to the threat of climate change,*
713 *sustainable development, and efforts to eradicate poverty* [V. Masson-Delmotte, P. Zhai, H. O. Pörtner,
714 D. Roberts, J. Skea, P. R. Shukla, A. Pirani, W. Moufouma-Okia, C. Péan, R. Pidcock, S. Connors, J. B.
715 R. Matthews, Y. Chen, X. Zhou, M. I. Gomis, E. Lonnoy, T. Maycock, M. Tignor, T. Waterfield (eds.)].
716 World Meteorological Organization, Geneva, Switzerland, 32 pp.
- 717 Jhajharia, D., Shrivastava, S. K., Sarkar, D., & Sarkar, S. (2009). Temporal characteristics of pan evaporation
718 trends under the humid conditions of northeast India. *Agricultural and Forest Meteorology*, 149(5), 763-
719 770. <https://doi.org/10.1016/j.agrformet.2008.10.024>

- 720 Jian, D., Li, X., Sun, H., Tao, H., Jiang, T., Su, B., & Hartmann, H. (2018). Estimation of Actual
721 Evapotranspiration by the Complementary Theory-Based Advection–Aridity Model in the Tarim River
722 Basin, China. *Journal of Hydrometeorology*, 19(2), 289-303. <https://doi.org/10.1175/jhm-d-16-0189.1>
- 723 Jun, A., Hideyukin K., & Lu M. (2004). Pan evaporation trends in Japan and its relevance to the variability of
724 the hydrological cycle. *Tenki*, 51(9), 667–678.
- 725 Kendall, M. G. (1975). *Rank correlation methods*. New York: Oxford University Press.
- 726 Lange, S. 2018. Bias correction of surface downwelling longwave and shortwave radiation for the EWEMBI
727 dataset. *Earth System Dynamics*. 9, 627–645. <https://doi.org/10.5194/esd-9-627-2018>
- 728 Lewis, S. C., King, A. D., & Mitchell, D. M. (2017). Australia's Unprecedented Future Temperature Extremes
729 Under Paris Limits to Warming. *Geophysical Research Letters*, 44(19), 9947-9956.
730 <https://doi.org/doi:10.1002/2017GL074612>
- 731 Li, Z., Zheng, F. L., & Liu, W. Z. (2012). Spatiotemporal characteristics of reference evapotranspiration during
732 1961–2009 and its projected changes during 2011–2099 on the Loess Plateau of China. *Agricultural and*
733 *Forest Meteorology*, 154–155, 147-155. <http://dx.doi.org/10.1016/j.agrformet.2011.10.019>
- 734 Liu, B., Xu, M., Henderson, M., & Gong, W. (2004). A spatial analysis of pan evaporation trends in China,
735 1955–2000. *Journal of Geophysical Research: Atmospheres*, 109(D15).
736 <https://doi.org/doi:10.1029/2004JD004511>
- 737 Liu, Q., Yang, Z., Cui, B., & Sun, T. (2010). The temporal trends of reference evapotranspiration and its
738 sensitivity to key meteorological variables in the Yellow River Basin, China. *Hydrological Processes*,
739 24(15), 2171-2181. <https://doi.org/doi:10.1002/hyp.7649>
- 740 Lv, M., Ma, Z., Yuan, X., Lv, M., Li, M., & Zheng, Z. (2017). Water budget closure based on GRACE
741 measurements and reconstructed evapotranspiration using GLDAS and water use data for two large
742 densely-populated mid-latitude basins. *Journal of Hydrology*, 547, 585-599.
743 <https://doi.org/10.1016/j.jhydrol.2017.02.027>
- 744 Lv, M. X., Ma, Z. G., Lv, M. Z. (2018). Effects of climate/land surface changes on streamflow with
745 consideration of precipitation intensity and catchment characteristics in the yellow river basin. *Journal of*
746 *Geophysical Research: Atmospheres*, 123(4), 1942-1958. <https://doi.org/doi:10.1002/2017JD027625>

- 747 Ma, Z. G. (2005). Historical regular patterns of the discharge in the Yellow River and the cause of their
748 formation (in Chinese). *Chinese Journal of Geophysics*, 48(6), 1270-1275.
749 <https://doi.org/10.3321/j.issn:0001-5733.2005.06.007>
- 750 Mann, H. B. (1945). Nonparametric tests against trend. *Econometrica: Journal of the Econometric Society*,
751 13(3), 245–259. <https://doi.org/10.2307/1907187>
- 752 McVicar, T. R., Li, L., Van Niel, T. G., Zhang, L., Li, R., Yang, Q., et al. (2007). Developing a decision
753 support tool for China's re-vegetation program: Simulating regional impacts of afforestation on average
754 annual streamflow in the Loess Plateau. *Forest Ecology and Management*, 251(1), 65-81.
755 <https://doi.org/10.1016/j.foreco.2007.06.025>
- 756 Mitchell, D., AchutaRao, K., Allen, M., Bethke, I., Beyerle, U., Ciavarella, A., et al. (2017). Half a degree
757 additional warming, prognosis and projected impacts (HAPPI): background and experimental design.
758 *Geoscientific Model Development*, 10(2), 571-583. <https://doi.org/10.5194/gmd-10-571-2017>
- 759 Mitchell, D., James, R., Forster, P. M., Betts, R. A., Shiogama, H., & Allen, M. (2016). Realizing the impacts
760 of a 1.5 [deg]C warmer world. *Nature Climate Change*, 6(8), 735-737.
761 <https://doi.org/10.1038/nclimate3055>
- 762 Paltineanu, C., Mihailescu, I. F., Prefac, Z., Dragota, C., Vasenciuc, F., & Claudia, N. (2008). Combining the
763 standardized precipitation index and climatic water deficit in characterizing droughts: a case study in
764 Romania. *Theoretical and Applied Climatology*, 97(3-4), 219-233. [https://doi.org/10.1007/s00704-008-](https://doi.org/10.1007/s00704-008-0061-1)
765 [0061-1](https://doi.org/10.1007/s00704-008-0061-1)
- 766 Paltineanu, C., Mihailescu, I. F., Seceleanu, I., Dragota, C., & Vasenciuc, F. (2007). Using aridity indices to
767 describe some climate and soil features in Eastern Europe: a Romanian case study. *Theoretical and*
768 *Applied Climatology*, 90(3-4), 263-274. <https://doi.org/10.1007/s00704-007-0295-3>
- 769 Peterson, T. C., Golubev, V. S., & Groisman, P. Y. (1995). Evaporation losing its strength. *Nature*, 377, 687.
770 <https://doi.org/10.1038/377687b0>
- 771 Roderick, M. L., & Farquhar, G. D. (2002). The Cause of Decreased Pan Evaporation over the Past 50 Years.
772 *Science*, 298(5597), 1410-1411. <https://doi.org/10.1126/science.1075390-a>

- 773 Roderick, M. L., & Farquhar, G. D. (2004). Changes in Australian pan evaporation from 1970 to 2002.
774 *International Journal of Climatology*, 24(9), 1077-1090. <https://doi.org/10.1002/joc.1061>
- 775 Roderick, M. L., Rotstayn, L. D., Farquhar, G. D., & Hobbins, M. T. (2007). On the attribution of changing
776 pan evaporation. *Geophysical Research Letters*, 34(17). <https://doi.org/10.1029/2007GL031166>
- 777 Ruane, A. C., Phillips, M. M., & Rosenzweig, C. (2018). Climate shifts within major agricultural seasons for
778 +1.5 and +2.0 °C worlds: HAPPI projections and AgMIP modeling scenarios. *Agricultural and Forest*
779 *Meteorology*, 259, 329-344. <https://doi.org/10.1016/j.agrformet.2018.05.013>
- 780 Schleussner, C. F., Deryng, D., Müller, C., Elliott, J., Saeed, F., Folberth, C., et al. (2018). Crop productivity
781 changes in 1.5 °C and 2 °C worlds under climate sensitivity uncertainty. *Environmental Research Letters*,
782 13(6), 064007. <https://doi.org/10.1088/1748-9326/aab63b>
- 783 Schleussner, C. F., Rogelj, J., Schaeffer, M., Lissner, T., Licker, R., Fischer, E. M., et al. (2016). Science and
784 policy characteristics of the Paris Agreement temperature goal. *Nature Climate Change*, 6(9), 827-835.
785 <https://doi.org/10.1038/nclimate3096>
- 786 Seneviratne, S. I., Wartenburger, R., Guillod, B. P., Hirsch, A. L., Vogel, M. M., Brovkin, V., et al. (2018).
787 Climate extremes, land–climate feedbacks and land-use forcing at 1.5°C. *Philosophical Transactions of*
788 *the Royal Society A: Mathematical, Physical and Engineering Sciences*, 376(2119).
789 <https://doi.org/10.1098/rsta.2016.0450>
- 790 She, D., & Xia, J. (2013). The spatial and temporal analysis of dry spells in the Yellow River basin, China.
791 *Stochastic Environmental Research and Risk Assessment*, 27(1), 29-42. [https://doi.org/10.1007/s00477-](https://doi.org/10.1007/s00477-011-0553-x)
792 [011-0553-x](https://doi.org/10.1007/s00477-011-0553-x)
- 793 Shi, H., & Shao, M. (2000). Soil and water loss from the Loess Plateau in China. *Journal of Arid*
794 *Environments*, 45(1), 9-20. <https://doi.org/10.1006/jare.1999.0618>
- 795 Shiau, J. T., Feng, S., & Nadarajah, S. (2007). Assessment of hydrological droughts for the Yellow River,
796 China, using copulas. *Hydrological Processes*, 21(16), 2157-2163. <https://doi.org/doi:10.1002/hyp.6400>
- 797 Su, B., Huang, J., Fischer, T., Wang, Y., Kundzewicz, Z. W., Zhai, J., et al. (2018). Drought losses in China
798 might double between the 1.5 °C and 2.0 °C warming. *Proceedings of the National Academy of Sciences*.
799 <https://doi.org/10.1073/pnas.1802129115>

- 800 Su, B., Huang, J., Gemmer, M., Jian, D., Tao, H., Jiang, T., & Zhao, C. (2016). Statistical downscaling of
801 CMIP5 multi-model ensemble for projected changes of climate in the Indus River Basin. *Atmospheric*
802 *Research*, 178-179, 138-149. <https://doi.org/10.1016/j.atmosres.2016.03.023>
- 803 Su, B., Jian, D., Li, X., Wang, Y., Wang, A., Wen, S., et al. (2017). Projection of actual evapotranspiration
804 using the COSMO-CLM regional climate model under global warming scenarios of 1.5°C and 2.0°C in
805 the Tarim River basin, China. *Atmospheric Research*, 196, 119-128.
806 <https://doi.org/10.1016/j.atmosres.2017.06.015>
- 807 Sun, Q., Miao, C., & Duan, Q. (2015). Projected changes in temperature and precipitation in ten river basins
808 over China in 21st century. *International Journal of Climatology*, 35(6), 1125-1141.
809 <https://doi.org/doi:10.1002/joc.4043>
- 810 Tang, K. L., Chen, Y. Z., & Jing, K. (1991). *Characteristics of soil erosion and its control on Loess Plateau*
811 *(in Chinese)*. Beijing: Science and technology of China press.
- 812 Taylor, K. E., Stouffer, R. J., & Meehl, G. A. (2012). An overview of CMIP5 and the experiment design.
813 *Bulletin of the American Meteorological Society*, 93(4), 485-498. <https://doi.org/10.1175/bams-d-11->
814 [00094.1](https://doi.org/10.1175/bams-d-11-00094.1)
- 815 Trenberth, K. E., Dai, A., van der Schrier, G., Jones, P. D., Barichivich, J., Briffa, K. R., & Sheffield, J.
816 (2013). Global warming and changes in drought. *Nature Climate Change*, 4, 17.
817 <https://doi.org/10.1038/nclimate2067>
- 818 Vicente-Serrano, S. M., Beguería, S., & López-Moreno, J. I. (2009). A Multiscalar Drought Index Sensitive to
819 Global Warming: The Standardized Precipitation Evapotranspiration Index. *Journal of Climate*, 23(7),
820 1696-1718. <https://doi.org/10.1175/2009JCLI2909.1>
- 821 Vicente-Serrano, S. M., Beguería, S., Lorenzo-Lacruz, J., Camarero, J. J., López-Moreno, J. I., Azorin-Molina,
822 C., et al. (2012). Performance of Drought Indices for Ecological, Agricultural, and Hydrological
823 Applications. *Earth Interactions*, 16(10), 1-27. <https://doi.org/10.1175/2012ei000434.1>
- 824 Vicente-Serrano, S. M., Van der Schrier, G., Beguería, S., Azorin-Molina, C., & Lopez-Moreno, J.-I. (2015).
825 Contribution of precipitation and reference evapotranspiration to drought indices under different climates.
826 *Journal of Hydrology*, 526, 42-54. <https://doi.org/https://doi.org/10.1016/j.jhydrol.2014.11.025>

- 827 Wang, W., Shao, Q., Peng, S., Xing, W., Yang, T., Luo, Y., et al. (2012). Reference evapotranspiration change
828 and the causes across the Yellow River Basin during 1957–2008 and their spatial and seasonal
829 differences. *Water Resources Research*, 48(5). <https://doi.org/doi:10.1029/2011WR010724>
- 830 Wang, Y., & Peng, S.M. (Eds.). (2017). *Principle and technology of drought monitoring and water resource*
831 *allocation in the Yellow River basin* (in Chinese). Beijing: Science press.
- 832 Wang, Y., Ding, Y., Ye, B., Liu, F., Wang, J., & Wang, J. (2013). Contributions of climate and human
833 activities to changes in runoff of the Yellow and Yangtze rivers from 1950 to 2008. *Science China Earth*
834 *Sciences*, 56(8), 1398-1412. <https://doi.org/10.1007/s11430-012-4505-1>
- 835 Wang, Z., Xie, P., Lai, C., Chen, X., Wu, X., Zeng, Z., & Li, J. (2017). Spatiotemporal variability of reference
836 evapotranspiration and contributing climatic factors in China during 1961–2013. *Journal of Hydrology*,
837 544, 97-108. <https://doi.org/10.1016/j.jhydrol.2016.11.021>
- 838 Wehner, M., Stone, D., Mitchell, D., Shiogama, H., Fischer, E., Graff, L. S., et al. (2018). Changes in
839 extremely hot days under stabilized 1.5 and 2.0 °C global warming scenarios as simulated by the HAPPI
840 multi-model ensemble. *Earth System Dynamics*, 9(1), 299-311. <https://doi.org/10.5194/esd-9-299-2018>
- 841 Xie, Y. G., & Fu, Q. (2004). Analysis of famines caused by heavy floods and droughts in China. *Nature and*
842 *Science*, 2 (2), 25–32.
- 843 Xu, C., & Singh, V. P. (2004). Review on Regional Water Resources Assessment Models under Stationary and
844 Changing Climate. *Water Resources Management*, 18(6), 591-612. [https://doi.org/10.1007/s11269-004-](https://doi.org/10.1007/s11269-004-9130-0)
845 9130-0
- 846 Xu, C., Gong, L., Jiang, T., Chen, D., & Singh, V. P. (2006). Analysis of spatial distribution and temporal
847 trend of reference evapotranspiration and pan evaporation in Changjiang (Yangtze River) catchment.
848 *Journal of Hydrology*, 327(1–2), 81-93. <http://dx.doi.org/10.1016/j.jhydrol.2005.11.029>
- 849 Yan, Y., Yang, Z., & Liu, Q. (2013). Nonlinear trend in streamflow and its response to climate change under
850 complex ecohydrological patterns in the Yellow River Basin, China. *Ecological Modelling*, 252, 220-227.
851 <https://doi.org/10.1016/j.ecolmodel.2012.05.022>

- 852 Yang, D., Li, C., Hu, H., Lei, Z., Yang, S., Kusuda, T., et al. (2004). Analysis of water resources variability in
853 the Yellow River of China during the last half century using historical data. *Water Resources Research*,
854 40(6). <https://doi.org/doi:10.1029/2003WR002763>
- 855 Yellow River Conservancy Commission of MWR (YRCC). (2007). *Yellow River water resources bulletin* (in
856 Chinese). Zhengzhou: Yellow River Conservancy Press.
- 857 Yellow River Conservancy Commission of MWR (YRCC). (2015). *Yellow River water resources bulletin* (in
858 Chinese). Zhengzhou: Yellow River Conservancy Press.
- 859 Zhai, R., Tao, F., & Xu, Z. (2018). Spatial–temporal changes in runoff and terrestrial ecosystem water
860 retention under 1.5 and 2 °C warming scenarios across China. *Earth System Dynamics*, 9(2), 717-738.
861 <https://doi.org/10.5194/esd-9-717-2018>
- 862 Zhang, Y., You, Q., Chen, C., & Ge, J. (2016). Impacts of climate change on streamflows under RCP
863 scenarios: A case study in Xin River Basin, China. *Atmospheric Research*, 178-179, 521-534.
864 <https://doi.org/10.1016/j.atmosres.2016.04.018>
- 865 Zhu, Z., Giordano, M., Cai, X., & Molden, D. (2004). The Yellow River Basin: Water Accounting, Water
866 Accounts, and Current Issues. *Water International*, 29(1), 2-10.
867 <https://doi.org/10.1080/02508060408691742>